Hydrology of malaria: Model development and application to a Sahelian village

Arne Bomblies,[1] Jean-Bernard Duchemin,[2] and Elfatih A. B. Eltahir[1]

Received 13 February 2008; revised 8 September 2008; accepted 29 September 2008; published 31 December 2008.

[1] We present a coupled hydrology and entomology model for the mechanistic simulation of local-scale response of malaria transmission to hydrological and climatological determinants in semiarid, desert fringe environments. The model is applied to the Sahel village of Banizoumbou, Niger, to predict interannual variability in malaria vector mosquito populations that lead to variations in malaria transmission. Using a high-resolution, small-scale distributed hydrology model that incorporates remotely sensed data for land cover and topography, we simulate the formation and persistence of the pools constituting the primary breeding habitat of *Anopheles gambiae s.l.* mosquitoes, the principal regional malaria vector mosquitoes. An agent-based mosquito population model is coupled to the distributed hydrology model, with aquatic-stage and adult-stage components. Through a dependence of aquatic-stage mosquito development and adult emergence on pool persistence, we model small-scale hydrology as a dominant control of mosquito abundance. For each individual adult mosquito, the model tracks attributes relevant to population dynamics and malaria transmission, which are updated as mosquitoes interact with their environment, humans, and animals. Weekly field observations were made in 2005 and 2006. A 16% increase in rainfall between the two years was accompanied by a 132% increase in mosquito abundance between 2005 and 2006. The model reproduces mosquito population variability at seasonal and interannual timescales and highlights individual pool persistence as a dominant control. Future developments of the presented model can be used in the evaluation of impacts of climate change on malaria, as well as the a priori evaluation of environmental management-based interventions.

Citation: Bomblies, A., J.-B. Duchemin, and E. A. B. Eltahir (2008), Hydrology of malaria: Model development and application to a Sahelian village, *Water Resour. Res.*, *44*, W12445, doi:10.1029/2008WR006917.

1. Introduction

1.1. Background

[2] Malaria is inextricably tied to water. Because malaria vector mosquitoes utilize water bodies for breeding, malaria cannot exist in regions where environmental conditions prohibit the formation and persistence of such water bodies. Consequently, for regions where water availability limits mosquito populations, hydrology models can provide useful predictive tools for vector mosquito population dynamics, which extends to malaria force of infection. Addressing the inherently cross-disciplinary nature of this problem using numerical modeling techniques at the appropriate spatial and temporal scales should result in an improved understanding of malaria transmission dynamics. We present such a model in this study, applicable to village-scale malaria transmission within African desert-fringe environments such as the Sahel. We then apply the model to Banizoumbou, a typical Sahelian village in southwestern Niger.

[3] Malaria burden is particularly severe in sub-Saharan Africa. Sixty percent of the world's 300–500 million clinical malaria cases and 80% of worldwide malaria deaths [*World Health Organization*, 2005] occur in this region. This disproportionately high disease burden in Africa is due primarily to the dominance of *Plasmodium falciparum*, the most severe and fatal form of human malaria, as well as behavioral traits of *Anopheles gambiae* mosquitoes, the principal vectors of the disease in much of the continent. *An. gambiae*'s strong preference for human hosts (anthropophily) makes it an exceedingly efficient vector [*White*, 1974; *Costantini et al.*, 1996a].

[4] In the African Sahel, monsoonal rainfall collects in small ephemeral pools which dot the landscape after rainfall events [*Desconnets et al.*, 1997]. These pools are the preferred breeding habitat of *An. gambiae*. Figure 1 shows an example of a typical anopheles-infested rainwater pool near Banizoumbou. In much of the Sahel, such pools are ubiquitous, and are often found to contain many mosquito larvae, especially near human habitation. The subset of these pools persisting long enough for at least one complete subadult mosquito maturation cycle (7–10 days) facilitates the observed explosive mosquito population growth during

[1] Ralph M. Parsons Laboratory, Massachusetts Institute of Technology, Cambridge, Massachusetts, USA.
[2] Centre de Recherche Médicale et Sanitaire, International Network of the Pasteur Institute, Niamey, Niger.

0043-1397/08/2008WR006917$09.00

Figure 1. A typical rain-fed pool that facilitates malaria mosquito breeding. Such pools dot the landscape and can become infested with mosquito larvae. They are the primary controls of population dynamics in the Sahel. Note the proximity to the village in the background.

the Sahel monsoon [*Gillies and DeMeillon*, 1968]. This seasonal mosquito population peak precedes and causes observed seasonal peaks in malaria incidence, which lag the wet season peaks by several weeks. Figure 2 shows malaria incidence data for 3 years at the clinics in Niger, superimposed on Global Precipitation Climatology Project monthly average rainfall in the same region. In this particular case malaria is endemic (constantly present) but highly seasonal. The dependence of malaria incidence and burden on seasonal precipitation-driven mosquito population dynamics is abundantly clear.

[5] Owing to the lower levels of natural immunity resulting from lack of year-round sustained malaria transmission, zones of unstable malaria transmission such as semiarid regions or transition zones between malaria-endemic and malaria-free regions are often subject to periodic severe malaria epidemics when environmental conditions shift to favor malaria transmission [*Kiszewski and Teklehaimanot*, 2004]. With its infamous climate variability, the Sahel is no exception. Because of this unstable and seasonally severe malaria transmission, we focus our effort on modeling environmental conditions typical of the Sahel as a forcing for a mosquito population model.

[6] In addition to precipitation-driven pool formation, environmental variables can affect the transmission of malaria in several ways. First, the temperature of water bodies (influenced by solar radiation, rainfall, and air temperature) governs the development rate of aquatic stages from eggs to adult emergence. After emergence, because mosquitoes cannot regulate their body temperature, ambient temperature sensed by the adult mosquito strongly affects gonotrophic (egg development) and sporogonic (sporozoite parasite stage development) rates in a degree-day dependence [*Detinova*, 1962]. Furthermore, relative humidity and temperature are thought to influence survivability of adult mosquitoes [*Clements*, 1963; *Craig et al.*, 1999]. Low relative humidity and high temperature may severely stress mosquitoes and cause premature death. The requirement that mosquito longevity exceed the temperature-dependent extrinsic incubation period (parasite development time within the mosquito before it can be transmitted to the next host) restricts malaria transmission to areas with conducive

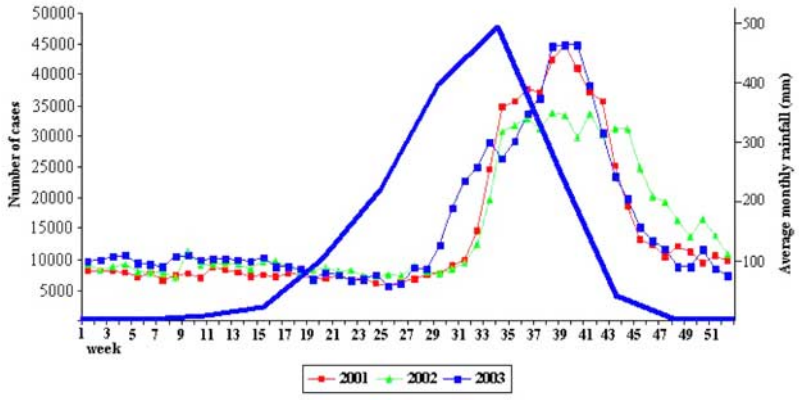

Figure 2. Weekly malaria incidence in Niamey, Niger, from 2001 to 2003, including Global Precipitation Climatology Project (GPCP) average monthly precipitation data.

climate conditions. In addition, small-scale variability in these variables associated with microhabitats (e.g., in houses, in tree canopies, or other such shelters) may provide refuges sought out by mosquitoes to escape highly stressful ambient conditions such as low humidity, high temperature, or high wind, and may influence survivability and vectorial capacity [*Okech et al.*, 2003]. Thus, actual mosquito longevity and sporogonic development may differ from those predicted by coarse-resolution models for mosquitoes occupying microhabitats. Malaria transmission and force of infection strongly depends on both mosquito longevity and sporogonic development [*Ross*, 1911; *Macdonald*, 1957].

[7] Spatial relationships between *Anopheles* breeding habitat, the vectors' human hosts, and favorable microhabitats can also significantly factor into transmission intensity of a human population. Flight distance between productive breeding sites and nearest human habitation can affect mosquito fecundity through lower time required for each gonotrophic cycle [*Le Menach et al.*, 2005; *Minakawa et al.*, 2002], and proximity of predicted breeding pools to sources of airborne nutriment such as maize pollen can strongly influence pool productivity [*Ye-Ebiyo et al.*, 2003].

[8] Mosquito population response to environmental perturbations such as climate variability is highly nonlinear. This is due not only to nonlinear hydrologic response to rainfall variability and the threshold temperature and humidity effects outlined above, but also to ecological limitations of nutrient competition and predation, which act in response to exponentially growing populations, in a negative feedback [*Sutherst*, 2004]. The combined effects from all of these factors suggest that simple correlative studies of malaria prevalence with climate variables may not suffice, and a more sophisticated approach is necessary in order to adequately predict system response to perturbation scenarios. The complex system of malaria's dependence on environmental conditions may be best studied using a representative mechanistic model.

[9] The presented model was developed for two primary goals. First, we seek to understand the effects of interannual climate variability on village-scale malaria transmission. Identification of the environmental factors driving seasonal transmission variability is a key to understanding longer-term trends in malaria transmission [*Pascual and Dobson*, 2005]. In the Sahel, anopheles breeding pool persistence (and therefore potential for mosquito breeding productivity) depends as much on precipitation frequency, timing and individual storm hyetographs as it does on cumulative rainfall. Excessive rainfall may flush out breeding pools, but storm return periods significantly longer than typical pool persistence times would result in pool desiccation, total sterilization of all aquatic-stage mosquitoes within that pool, and would therefore preclude adult mosquito development [*Charlwood et al.*, 1995]. Site-specific microtopography, microclimate, and soil and vegetation type determine pool persistence. Interannual variability in humidity and temperature can affect populations as well, as described above. The model was developed to address effects of the Sahel's pronounced climate variability on malaria transmission and transmissibility, measured by malaria prevalence and mosquito vectorial capacity. Future applications of the coupled model can evaluate effects of climate change on malaria transmission. Accurate forecasts may be limited by the model's inability to simulate human adaptation to long-term climate change, but the mechanisms for evaluating climate change effects on malaria transmission in a stable, stationary population are built into the model.

[10] The second purpose of the coupled model development was to construct a modeling framework that allows explicit representation of the spatial determinants of malaria transmission. Differences in pool productivities may be related to a variety of proximal factors, all of which have small characteristic scales, such as nearby human habitation, presence of livestock (which act as an alternate blood meal source for anophelines), nearby pollen sources such as maize or millet or microhabitat availability. Mosquitoes' interactions with these spatial determinants and the village inhabitants can be represented using an agent-based approach operating on a small-scale grid. Spatial structure of the population is maintained, which is absent in analytical models with ''perfect mixing'' assumptions. With such a format, mosquito population structure can be reproduced, observed, and studied in a simulated, virtual field environment. An important extension of this design purpose is that potential local intervention methodologies can be evaluated a priori. The model can evaluate a variety of environmental management scenarios, such as the effects of pool removal, draining, larviciding, etc. In addition, specific questions about mosquito population behavior such as dry season survival, or intervillage mosquito migrations can be examined.

[11] Several studies have confirmed association of climate variability and malaria transmission, and some models have demonstrated predictive ability based on malaria/climate associations using past observations [e.g., *Teklehaimanot et al.*, 2004; *Thomson et al.*, 2006]. However, with an associative approach and a coarse spatial scale, these types of models cannot fully untangle the complexities of malaria dependence on environmental variables, and thus may not provide adequate predictive ability to test climate change or intense climate variability scenarios. In addition, because small-scale spatial variations in soil, vegetation type and especially topography influence the degree of pooling for a given rainfall amount, coarse resolution models may be limited in applicability [*Thomson et al.*, 2004]. Resolution must be adequately high in order to predict precipitation effects on *Anopheles gambiae* mosquito ecology in the Sahel. *Shaman et al.* [2002] demonstrated that high-resolution soil moisture modeling that incorporates topographic details yields good correlation of soil moisture states with captured mosquito abundances in New Jersey. However, improvements on malaria models that are based largely on correlations with mosquito abundances or historical incidence data can be made with a mechanistic, first-principle simulation of environment-dependent processes involved, operating at appropriate scales. This should yield predictive ability for response to perturbations beyond the limits of past observations, such as extreme climate variability or climate change. For such a model, hydrology and entomology simulators are necessary intermediates.

[12] We evaluate the effects of climate variability on malaria transmissibility in the Sahel using the presented coupled hydrology/entomology model, forced with 2005 and 2006 field data. The application of this model to Banizoumbou, Niger, will demonstrate the model's utility

for studying malaria transmission responses to environmental variability.

1.2. Study Area

[13] Banizoumbou is a village in southwestern Niger (13° 31′, 2° 39′) of about 1000 inhabitants and is located in a semiarid plateau landscape of tiger bush, millet fields, fallow, and bare soil. Land use and land cover types in Banizoumbou's immediate environs are typical for Niger Sahelian villages. Average annual rainfall in nearby Niamey is 562 mm over the period 1905–1989 [*Le Barbé and Lebel*, 1997], all of which falls during the single May to October rain season with a peak in August. Because of extended drought, during the period 1968–1990, the average annual precipitation has decreased to 495 mm [*Le Barbé and Lebel*, 1997]. Average annual rainfall in recent years in Banizoumbou is slightly less at 450 mm. The majority of the annual rainfall occurs during the West African monsoon peak between mid-July and late August. The rain tends to fall at a high rate, with a distinctive hyetograph shape consisting of an initial burst of high-intensity and short-duration rain (squall line), followed by several hours of low-intensity rainfall from the trailing stratiform [*Amani and Lebel*, 1996].

[14] Regional topography as seen in digital elevation models reveals an extensive drainage network. However, these channels no longer conduct runoff, as they are relics from a wetter period [*Talbot*, 1980]. Pleistocene aeolian sand deposits in the drainages impound water in the channels [*Peugeot et al.*, 2003], confining runoff to small closed-basin catchments, which are typically no more than 1 km in length [*Desconnets et al.*, 1997]. Surrounding Banizoumbou, small catchments drain into pools several meters to tens of meters across [*Desconnets et al.*, 1997]. Pool inflows are balanced by a change in volume, infiltration, and evaporation, and levels fluctuate in response to inflows from concentrated runoff. Incidentally, infiltration from these pools is the primary source of recharge to the unconfined aquifer [*Leduc et al.*, 2001]. A layer of low-permeability clayey soil lines the bottom of these pools [*Desconnets et al.*, 1997]. Outside of the pools, homogenous sandy soils with 10–15% fine particle content predominate in the hillslopes and valley bottom ravines, and infiltration capacity in these sandy soils can reach 45 cm/h [*Peugeot et al.*, 2003]; however, the soils are highly susceptible to crust formation [*Hoogmoed and Stroosnijder*, 1984]. When crust forms, runoff coefficients can increase to 90%, with dramatic consequences for pool inflows [*Casenave and Valentin*, 1992].

[15] Subsistence dry-land agriculture dominates food production, and local vegetation consists primarily of millet fields near the village. Most of the land is farmed, some areas are left fallow, and the remainder consists of tiger bush shrubland, which is generally more distant from the village and is common near surrounding plateau tops. Banizoumbou villagers farm pearl millet almost exclusively, with small plots of beans, groundnuts, and other crops making up an insignificant portion of the cultivated land.

[16] As previously stated, *Anopheles gambiae s.s.* and *Anopheles arabiensis* mosquitoes dominate malaria transmission in Banizoumbou [*White*, 1974; J.-B. Duchemin, personal communication, 2005]. Both of these species are members of the *Anopheles gambiae s.l.* species complex, genus *Anopheles* (the only mosquito genus capable of transmitting malaria) [*Gillies and DeMeillon*, 1968]. The strong anthropophily (human-biting nature) of *Anopheles gambiae s.l.* mosquitoes makes them highly efficient malaria vectors [*White*, 1974; *Coluzzi et al.*, 1979; *Costantini et al.*, 1998]. The less abundant (and less anthropophilic) *Anopheles* species such as *An. pharoensis* and *An. rufipes* play only a very minor role in Banizoumbou malaria transmission [*Muriu et al.*, 2008; *Appawu et al.*, 2004]. The highly anthropophilic vector *Anopheles funestus* has never been captured in Banizoumbou and is assumed absent.

2. Model Development

[17] The presented model was developed to evaluate the aforementioned complexities in mosquito population response to climate variables in the Sahel, simulating breeding pool formation and persistence with a distributed hydrology model. Previous hydrology models have successfully correlated soil moisture and mosquito abundance. For example, *Patz et al.* [1998] showed an improved explanation of variance in *An. gambiae* abundance and biting in Western Kenya using modeled soil moisture, compared to both rainfall alone and normalized difference vegetation index (NDVI). Potential for the use of hydrologic modeling to predict malaria transmission was demonstrated with this study, however the spatial and temporal resolutions used in the model were low. Improvements on the use of a soil moisture model to predict mosquito abundance were made by *Shaman et al.* [2002]. As previously mentioned, they predicted distributed soil moisture at high spatial and temporal resolution in New Jersey, to correlate with observed abundances of mosquito species *Aedes vexans*, *Anopheles walkeri*, and *Culex pipiens*. *Ahumada et al.* [2004] developed a model to predict population dynamics of *Cx. quinquefasciatus* in Hawaii, as a function of seasonal changes in environmental conditions. These authors successfully predicted temporal population patterns along an altitudinal gradient. *Depinay et al.* [2004] and *Pascual et al.* [2006] incorporated temperature-dependent subadult development rates into mosquito population models. We use these prior studies as a foundation for our model development. However, we explicitly represent the distributed pooled water that constitutes anopheles mosquito breeding habitat as well as the soil moisture which governs the formation of this habitat, and link the resulting pooled water locations with a high temporal resolution individual-based representation of mosquito populations interacting with the environment.

[18] Figure 3 shows the conceptual schematic and coupling of various model components. Because spatial distributions of pools relative to human habitation are so important and can play a large role in transmission intensity [*Le Menach et al.*, 2005; *Minakawa et al.*, 1999; *Minakawa et al.*, 2002], a gridded region surrounding human habitation forms the model domain and individual pool locations are predicted using fine-scale topography as hydrology model input. Simulated pools in topographic depressions host subadult mosquitoes, which emerge as individual "agents" if their host pool persists long enough, and are free to interact with their simulated environment within the model domain based on a set of preassigned rules and attributes.

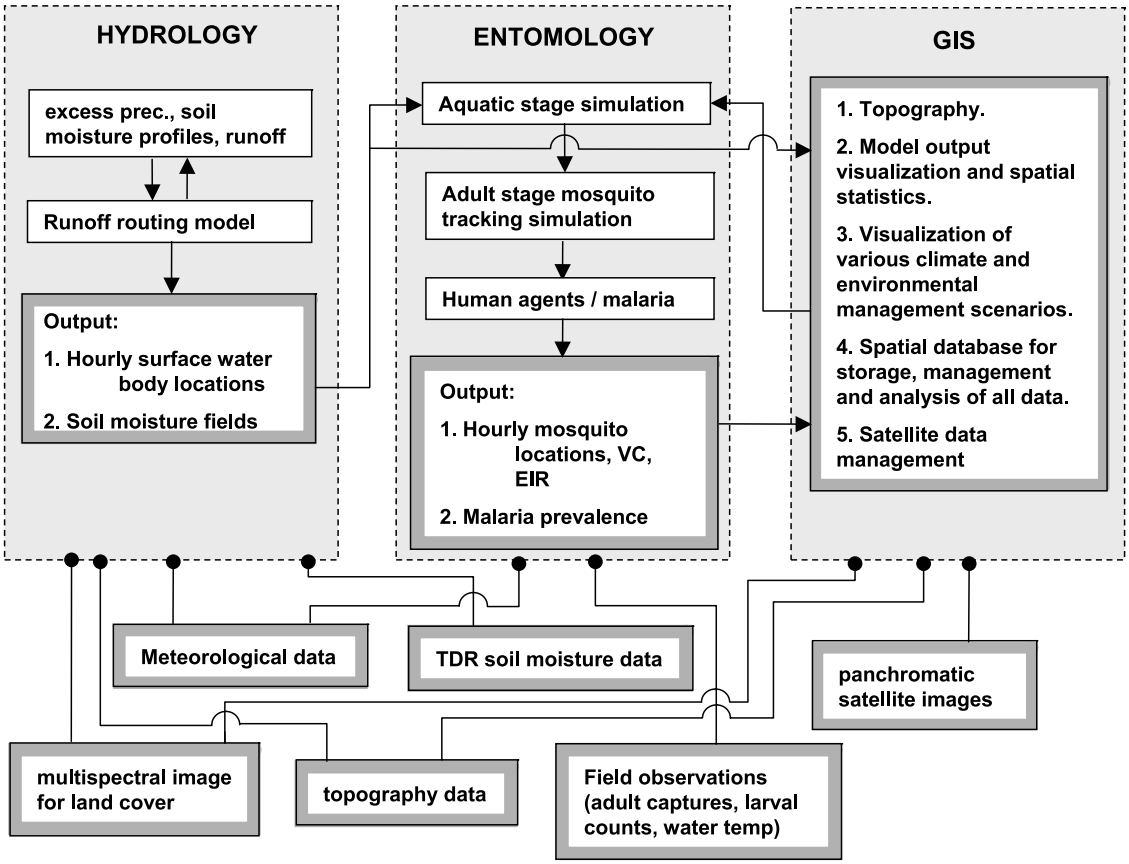

Figure 3. Schematic diagram of model setup, with three components. Various inputs into the different components are summarized in the bottom of the diagram. TDR, time domain reflectometry. VC, vectorial capacity. EIR, entomological inoculation rate.

[19] Pool persistence is a key mosquito population control. To inform the presented model, many field observations were made in a region of southwestern Niger considered representative of the Sahel. In this field environment, rain-fed pools and their entomological activity were monitored regularly. Pool desiccation kills all aquatic-stage mosquitoes [*Charlwood et al.*, 1995]. If they manage to emerge before desiccation, however, mosquitoes will plague humans living nearby. Interaction of simulated mosquito "agents" with immobile human agents facilitates virtual malaria transmission. A geographic information system (third component in the Figure 3 schematic) aids the visualization and management of model input and output.

2.1. Hydrology Model Development

2.1.1. Domain and Scale

[20] In the Sahel, the ephemeral pools that *An. gambiae* typically exploits for breeding are fed by closed basin catchments of less than 1-km flow length. The resulting pool sizes are typically tens of meters in diameter [*Desconnets et al.*, 1997]. In this region, *An. gambiae* exploits these medium-sized pools almost exclusively [*Service*, 1993]. Many references indicate that *An. gambiae* breeds prolifically in very small puddles such as cattle hoofprints [e.g., *Minakawa et al.*, 2004; *Mutuku et al.*, 2006; *Service*, 1993]. While larvae are indeed found in cattle hoofprints in the study area (considered representative of the Sahel), when filled with water these anopheline hoofprints are always directly within a larger-scale topographic depression which collects water, and as such are embodied by the presented model. Hoofprints distant from these topographic depressions never contain water long enough to allow subadult mosquito maturation. There is therefore no need to simulate at scales consistent with animal hoofprints for simulations in the arid Sahel. Moreover, anthropogenic water bodies such as discarded tires, small cans, water storage containers, discarded calabashes, or any other such container do not constitute *An. gambiae* habitat [*Service*, 1993]. While these tiny water bodies have been implicated in the breeding of yellow-fever vector *Aedes* mosquitoes, the local Anopheles mosquitoes virtually never oviposit (lay eggs) there. The same is true for deep wells.

[21] Studies of mosquito dispersal surrounding Sahel villages using marked release and recapture experiments have shown *An. gambiae* populations to cluster around these villages [*Gillies*, 1961; *Costantini et al.*, 1996b; *Taylor et al.*, 2001], from which some mosquitoes will stray from the village and enter neighboring villages [*Costantini et al.*, 1996b; *Taylor et al.*, 2001]. *An. gambiae* dispersal behavior and Sahelian hydrologic characteristics suggest appropriate model domain dimensions of several kilometers square surrounding villages or human populations of inter-

est and a resolution of 10 m. The presented model allows flexible, user-prescribed fine spatial discretization directly surrounding the population of interest for detailed pool resolution, and coarser resolutions away from pool locations in a telescopic mesh refinement. Coarse discretization at the pool catchments' upper reaches allows efficient and adequate overland flow simulation. The existence of small-scale pools in distant areas is not expected to influence significantly the village anopheline population, and therefore provides an acceptable compromise, which allows both satisfactory overland flow simulation and feasible run times.

2.1.2. Overland Flow

[22] Pool formation is simulated by distributed flow routing. A finite difference solution of a diffusion wave approximation to the St. Venant equations determines routed and pooled water for each time step. Run-on onto downgradient grid cells combines with available precipitation for the next iteration of the unsaturated zone model. In this manner, shallow flow over a spatially variable infiltrating surface is simulated. Flow velocity is represented by Manning's equation with distributed roughness parameter n. The formulation follows that of *Lal* [1998]. The continuity equation for shallow flow is

$$\frac{\partial h}{\partial t}+\frac{\partial (hu)}{\partial x}+\frac{\partial (hv)}{\partial y}-P+I+ET=0, \tag{1}$$

where u and v are the flow velocities in the x and y directions, respectively, h is the water depth, P is precipitation, I is infiltration, and ET is evapotranspiration.

[23] The momentum equations for the x and y directions are

$$\frac{\partial (hu)}{\partial t}+\frac{\partial (u^2h)}{\partial x}+\frac{\partial (uvh)}{\partial y}+hg\frac{\partial (h+z)}{\partial x}+ghS_{fx}=0, \tag{2}$$

$$\frac{\partial (hv)}{\partial t}+\frac{\partial (v^2h)}{\partial y}+\frac{\partial (uvh)}{\partial x}+hg\frac{\partial (h+z)}{\partial y}+ghS_{fy}=0, \tag{3}$$

where g is the gravitational acceleration, and S_{fx} and S_{fy} are the friction slopes in the x and y directions, respectively. For the diffusion wave approximation, we neglect the first three terms, which represent inertial effects. We make the replacement H = h + z for water level above a datum. Equations (2) and (3) then reduce to

$$\frac{\partial H}{\partial x}=-S_{fx}, \tag{4}$$

$$\frac{\partial H}{\partial y}=-S_{fy}. \tag{5}$$

Manning's equation relates flow velocity to friction slope and flow depth. For the x direction,

$$u=\frac{1}{n}h^{\frac{2}{3}}S_{fx}^{\frac{1}{2}}, \tag{6}$$

where n is the Manning's roughness coefficient which determines resistance to overland flow. The y direction velocity is formulated similarly. Following *Lal* [1998], we reformulate equation (6) in terms of H and n:

$$u=-\frac{h^{\frac{2}{3}}}{n\sqrt{S_{fx}}}\frac{\partial H}{\partial x}=-\frac{K}{h}\frac{\partial H}{\partial x}, \tag{7}$$

$$v=-\frac{h^{\frac{2}{3}}}{n\sqrt{S_{fy}}}\frac{\partial H}{\partial y}=-\frac{K}{h}\frac{\partial H}{\partial y}, \tag{8}$$

with $K=\frac{h^{\frac{5}{3}}}{n\sqrt{S_f}}$.

[24] Equations (1), (4), (5), (7), and (8) are then solved using the alternate-direction implicit (ADI) method. *Lal* [1998] found ADI to be the most efficient solver of several common options. At half time steps, the following equations are evaluated sequentially:

$$H_{i,j}^{*}=H_{i,j}^{n}+\frac{\Delta t}{\Delta A}\left[K_{i+1/2,j}\left(H_{i+1,j}^{*}-H_{i,j}^{*}\right)+K_{i-1/2,j}\left(H_{i-1,j}^{*}-H_{i,j}^{*}\right)\right]+\frac{\Delta t}{\Delta A}\left[K_{i,j+1/2}\left(H_{i,j+1}^{n}-H_{i,j}^{n}\right)+K_{i,j-1/2}\left(H_{i,j-1}^{n}-H_{i,j}^{n}\right)\right]+P, \tag{9}$$

$$H_{i,j}^{n+1}=H_{i,j}^{*}+\frac{\Delta t}{\Delta A}\left[K_{i+1/2,j}\left(H_{i+1,j}^{*}-H_{i,j}^{*}\right)+K_{i-1/2,j}\left(H_{i-1,j}^{*}-H_{i,j}^{*}\right)\right]+\frac{\Delta t}{\Delta A}\left[K_{i,j+1/2}\left(H_{i,j+1}^{n+1}-H_{i,j}^{n+1}\right)+K_{i,j-1/2}\left(H_{i,j-1}^{n+1}-H_{i,j}^{n+1}\right)\right]+P. \tag{10}$$

ΔA is the grid cell area, or $\Delta x\Delta y$. $H_{i,j}^{n}$ is the flow depth at the previous time step, $H_{i,j}^{*}$ is the flow depth at a half time step, and $H_{i,j}^{n+1}$ is the updated flow depth after both x and y directions are solved implicitly. Δt in this formulation is half of the model time step. Infiltration and evapotranspiration are left out of this formulation because they are updated in the unsaturated zone model, in a separate model subroutine.

[25] Topography at very high resolution is a critical parameter for overland flow simulation and prediction of pool formation. Topography determines the cell-to-cell bed slope, which is then used to determine intercell flow potentials [*Lal*, 1998]. The model uses a digital elevation model (DEM) that was derived from a combination of a ground topographic survey and Envisat synthetic aperture radar data [*Toutin and Gray*, 2000]. In addition to topography, Manning's n in equation (6) strongly controls the timing and volume of hydrographs entering topographic depressions. This roughness parameter depends on the vegetation cover and soil type at the grid cell, and influences overland flow velocities.

2.1.3. Land Surface Scheme

[26] The model presented borrows heavily from the land surface scheme LSX of *Pollard and Thompson* [1995]. The model simulates six soil layers and two vegetation layers for a detailed representation of hydrologic processes in the vertical column. LSX simulates momentum, energy, and water fluxes between the vegetation layers, soil, and the atmosphere. Vegetation type and soil type strongly influence soil moisture profile simulation, and spatially variable

Table 1. Hydrology Model Inputs

Variable	Type	Remarks
Vegetation	distributed	supervised classification of multispectral satellite image (e.g., Landsat)
Roughness	distributed	assigned on the basis of vegetation classification
Soil type	distributed	supervised classification and knowledge of local soil compositions
Topography	distributed	synthetic aperture radar products (e.g., Radarsat) or other suitable digital elevation model source
Precipitation	lumped	from meteorological station or climate model output
Temperature	lumped	from meteorological station or climate model output
Humidity	lumped	from meteorological station or climate model output
Wind speed	lumped	from meteorological station or climate model output
Wind direction	lumped	from meteorological station or climate model output
SW radiation	lumped	from meteorological station or climate model output
Grid resolution	user-defined	flexible telescopic mesh refinement grid layout to accommodate area of interest
Time step	user-defined	different time steps as input for overland flow and unsaturated zone models

soil and vegetation properties are used to assign roughness in the runoff routing model. Spatial variability of soil properties is a key determinant of the endorheic behavior observed in typical Sahel catchments [*Peugeot et al.*, 2003].

[27] Vertical soil layer thicknesses are assigned to allow simulation of a low-permeability structural crust commonly observed at the land surface in bare soil and sparsely vegetated areas of the Sahel [*d'Herbès and Valentin*, 1997]. Precipitation at each grid cell is partitioned between runoff and infiltration, on the basis of Hortonian runoff processes. The resulting infiltration flux is redistributed in the unsaturated zone with a Richards equation solver, with soil hydraulic parameters assigned for each layer and grid cell. The Richards equation governs vertical water movement through the unsaturated zone, for which the model uses an implicit solver. The Richards equation is

$$\frac{\partial\theta(z,t)}{\partial t} = \frac{\partial}{\partial z}\left[K_u(\theta)\frac{\partial\phi(\theta,z)}{\partial z} + K_u(\theta)\right] \tag{11}$$

where θ is soil moisture [$cm^3\ cm^{-3}$], $K_u(\theta)$ is unsaturated hydraulic conductivity [$m\ s^{-1}$], $\varphi(\theta,z)$ is head value [m], and z is elevation [m].

[28] Several key hydrologic parameters govern the rainfall partitioning into infiltration and runoff. Saturated hydraulic conductivity and porosity are two critical parameters. The soil model subroutine determines unsaturated zone hydraulic conductivity as a function of soil moisture following Campbell's equation [*Campbell*, 1985]:

$$K(\theta) = K_s\left(\frac{\theta}{\theta_s}\right)^{2b+3}, \tag{12}$$

where θ is the volumetric water content, and θ_s is the volumetric water content at saturation, (porosity) b is a model exponent dependent on soil texture, and K_s is the saturated hydraulic conductivity. The b exponent is introduced in this formulation as a model parameter, and derives from the moisture release equation [*Campbell and Norman*, 1998]:

$$\psi_m = \psi_e\left(\frac{\theta}{\theta_s}\right)^{-b}, \tag{13}$$

where ψ_m is the matric potential and ψ_e is the air entry potential. Air entry potential and b exponent are two soil parameters which influence unsaturated zone water redistribution, and nominal values are thus assigned on the basis of the observed soil texture in the field following Table 9.1 of *Campbell and Norman* [1998]. In addition, root zone soil water uptake from transpiration is forced by canopy-level climatic variables.

2.1.4. Model Inputs

[29] Necessary model inputs come from a variety of sources. The climate data for model forcing can come from meteorological stations in the field, and/or from regional climate model simulations. Meteorologic variable inputs for the hydrology model are temperature and humidity, wind speed and direction, incoming solar radiation, and precipitation. These six variables can be assumed spatially invariant over the model domain or can be represented as distributed rasters, on the basis of either multiple measurements or assumptions, to account for the existence of mosquito microhabitats. Table 1 summarizes all hydrology model inputs.

2.1.5. Model Operation

[30] The hydrology model operates according to the schematic shown in Figure 3. The overland flow module operates at a small user-defined time step (nominally 1 s), while the unsaturated zone model is stepped at a coarser time step (nominally 1 h). Vegetation canopy energy and water redistribution calculations are performed at this time step as well. The vegetation module tracks evapotranspiration and root zone moisture uptake for the various vegetation types. This interacts with the model's soil water redistribution component, which tracks both soil moisture and temperature in the vertical column. Routed water depths from the overland flow module are updated for infiltration and evapotranspiration losses at each model time step before being returned to the overland flow routing subroutine.

2.1.6. Model Output

[31] Pool depth rasters generated at each model time step (nominally 1 h) serve as entomology model input. The loosely coupled model structure derives from the one-way dependence of entomology on hydrology, as well as the need to calibrate the model components separately. Each output file contains water depths for each model grid cell, based on the user-prescribed grid configuration. Soil mois-

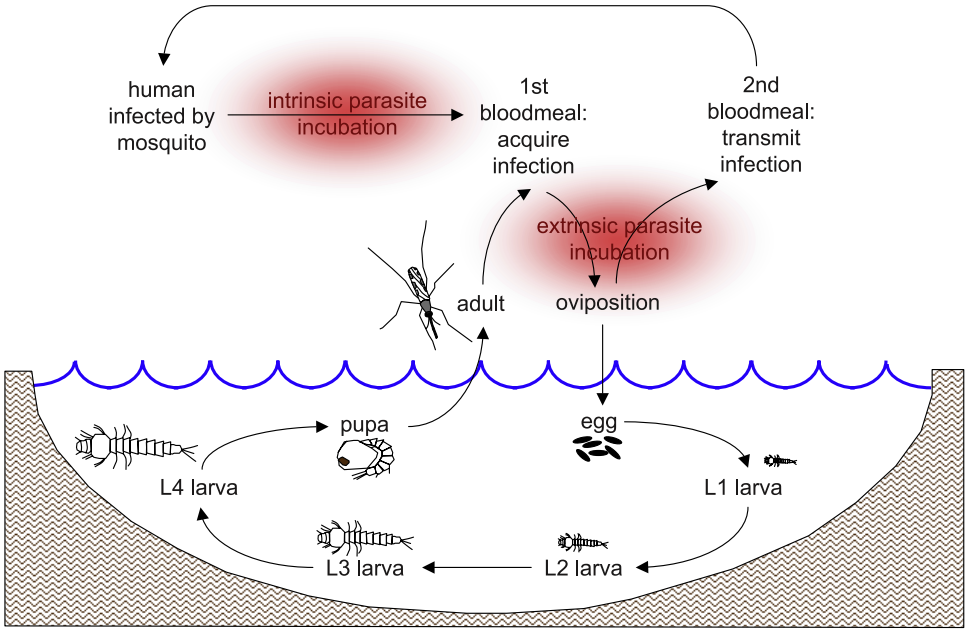

Figure 4. Advancement of aquatic stages of mosquitoes, from eggs to different stages of larvae, to pupae, and finally to adult emergence. The parasite enters the mosquito's body at the first infectious blood meal, which it uses to develop and deposit its first clutch of eggs. Parasite development continues with a degree-day dependence until the mosquito becomes infectious to humans. Transmission occurs when the infectious mosquito takes a second blood meal from a different human. Then, the parasite's intrinsic incubation period begins within the human body. A new mosquito takes a blood meal following the intrinsic incubation period and becomes infectious to repeat the transmission cycle.

ture profiles are tracked for each grid cell. Volumetric water content time series for user-specified points are also generated as output to allow hydrology model validation using profile soil moisture measurements such as time domain reflectometry (TDR) probes.

2.2. Entomology Model Development

[32] Malaria response to environmental determinants is simulated using individual mosquito and human "agents." Mobile individual mosquito agents behave probabilistically according to a prescribed set of rules governing dispersal and discrete events (e.g., blood meals, egg laying, etc.), in response to their immediate environment. This formulation allows population behavior of both mosquitoes and malaria parasites to emerge on the basis of the individuals' actions. Characteristics of each mosquito such as location and gonotrophic or infective status are tracked through time. At least two bites are required for a new malaria infection, one for the mosquito to acquire the parasite from an infected human, and a second bite from an uninfected human to cause the secondary infection (see Figure 4). Interaction with the human population, acquisition of infection, intrinsic and extrinsic incubation periods (parasite development time in humans and mosquitoes, respectively), and infectious bites upon subsequent contact with humans are all simulated in the described manner. Only female mosquitoes are tracked, because male mosquitoes do not take blood meals and therefore play no role in malaria transmission. We assume that male availability for mating is not limiting.

2.2.1. Model Input

[33] Model input for the entomology component includes pool water levels from the hydrology model output, as well as local meteorological conditions, if they are set to vary spatially. Certain aspects of mosquito behavior depend on relative humidity and temperature, and mosquito dispersal is influenced by wind speed and direction, both for physical displacement when wind is very strong, as well as to direct plumes of CO_2 and human odor from the villages which act as host-seeking cues [*Healy and Copland*, 1995; *Takken and Knols*, 1999]. CO_2-mediated flight behavior is described below. In addition, aquatic-stage development rates for the subadult mosquitoes depend on water temperatures [*Depinay et al.*, 2004]. Egg development within an adult mosquito, as well as the sporozoite phase of the *plasmodium* parasite, depend on ambient temperature [*Detinova*, 1962; *Craig et al.*, 1999]. Accordingly, these six variables (air temperature, water temperature, humidity, wind speed, wind direction, and distributed water depths) are the primary inputs for the entomology model. Water depth and temperature for each grid cell are predicted by the hydrology model, and the remaining four can be either field measured or supplied by climate models.

[34] The entomology model input variables temperature and humidity can be either spatially invariant throughout the domain, or can be distributed to allow simulation of microhabitats potentially inhabited by mosquitoes. These microhabitats, possibly under shady trees or in houses, can offer comfortable refuges to mosquitoes as an alternative to harsh ambient conditions. The less stressful conditions of suitable microhabitats can decrease mortality and temperature variations and can influence the parasite extrinsic incubation period [*Okech et al.*, 2003]. Both of these relevant microhabitat-related processes can affect village-scale malaria

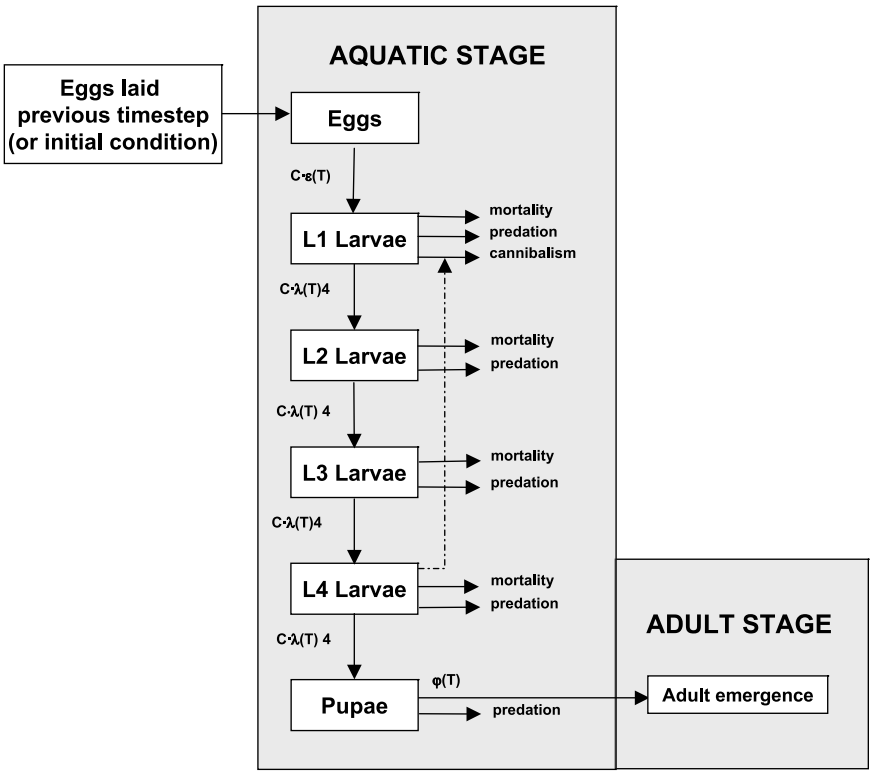

Figure 5. Aquatic-stage schematic diagram. ε(T) is a temperature-dependent egg development rate, λ(T) is the larvae development rate, ϕ(T) is the pupae development rate, and C is a coefficient to account for intraspecific nutrient competition.

transmission. Assignment of distributed temperature and humidity values can be done on the basis of remotely sensed land cover types. However, in the model application presented here, they are assumed spatially invariant.

2.2.2. Aquatic-Stage Simulation

[35] Aquatic-stage, or subadult, mosquitoes advance through several stages between eggs and adult mosquitoes. As shown in Figure 4, eggs hatch to become L1, or first-stage larvae. They then advance through three more larval stages (instars) as they grow and mature, to finally pupate. Pupae do not feed. They remain in this state for approximately two days before emerging as adult mosquitoes.

[36] Simulation of aquatic-stage development relies on a compartmental structure model for each grid cell in which the hydrology model assigns a pool. As long as the pool persists in the simulation, the aquatic-stage model will continue to advance. In pools predicted by the hydrology model to disappear, any simulated aquatic stages will be killed in the simulation, as is expected of naturally occurring *An. gambiae* larvae and pupae upon desiccation [*Charlwood et al.*, 1995]. Figure 5 presents the aquatic-stage model structure, which is embedded within each model grid cell containing water. This model describes the water temperature-dependent stage progression rates of eggs, larvae, pupae, and emerging adults. Only integer abundances are advanced from a previous stage to the next. Temperature dependence of the progression rates has been observed by *Bayoh and Lindsay* [2004] and incorporated in the model of *Depinay et al.* [2004]. During each model time step, in pools with subadult mosquitoes, the progression from eggs to larvae to pupae to adults is calculated using Depinay's temperature-dependent model:

$$d_k = r(T_k) \cdot \Delta t_k, \tag{14}$$

where d is the fraction of individuals in a certain stage progressed to the next stage, T_k is the temperature (K) over time interval k, Δt_k is the time step at interval k, and $r(T_k)$ is the temperature-dependent development rate, given by *Depinay et al.* [2004] as a function of water temperature and biochemical parameters specific to each subadult stage. For details of the temperature dependence, the reader is referred to the work of *Depinay et al.* [2004].

[37] As shown in Figure 5, each larval instar (L1 through L4) is subject to predation and natural mortality losses. In addition, L4 larvae cannibalize L1 larvae at a rate dependent on L4 larvae abundance [*Koenraadt and Takken*, 2003]. For all stages, predation and natural mortality are model parameters. Pupae are subject to predation losses, but we assume that they do not suffer natural mortality. The development rates between the aquatic stages (ε(T), λ(T), and φ(T) for egg, larvae and pupae, respectively, as in Figure 5) are represented by r(T) in equation (14).

[38] Following *Depinay et al.* [2004], we limit pool biomass using the ecological carrying capacity, which becomes a model parameter. As an example of nutrient limitations, in past studies mosquito larval abundance and pool productivity has been highly correlated to availability of maize pollen [*Ye-Ebiyo et al.*, 2003]. In Figure 5, the coefficient C represents competition for limited nutrients in each pool, restricting advancement as the pool biomass

Table 2. Mosquito Attribute Matrix

Number	Name	Remarks
1	mosquito ID number	constant throughout simulation
2	X position of mosquito	weighted radial random walk; determined from a number of anthropological and meteorological tropisms
3	Y position of mosquito	weighted radial random walk; determined from a number of anthropological and meteorological tropisms
4	elapsed time since emergence	Δt added each time step
5	blood meal flag	= 1 for blood meal; 0 otherwise
6	elapsed time since blood meal	Δt added each time step after blood meal
7	oviposition flag	add 1 each time mosquito oviposits
8	elapsed time since oviposition	Δt added each time step after oviposition
9	death flag	= 1 if death occurs; 0 otherwise
10	infection flag	= 1 if mosquito becomes infected; 0 otherwise
11	degree days since infection	updated each time step

approaches the assigned carrying capacity. As in Depinay's model, an intraspecific competition coefficient is defined as

$$C = \left(\frac{e - w}{e}\right), \tag{15}$$

where w is the sum of total larval biomass in the pool grid cell, and e is the ecological carrying capacity [mg biomass m^{-2}]. Ecological carrying capacity is an assigned model parameter and is assumed to be time invariant.

[39] Several other factors influence larvae. Pool water temperatures in excess of 40 degrees result in death of larvae [*Jepson et al.*, 1947; *Depinay et al.*, 2004]. In addition, we assume that oviposition does not occur in pools deeper than a threshold depth [*Minakawa et al.*, 2005]. This is consistent with our own observations that wave action (which generally occurs in deeper, larger, unvegetated pools) seems to deter larvae, either by wave action drowning them or by waves discouraging oviposition. Also, deep water in the center of large pools appears to contain virtually no larvae. In the hydrology simulation, shrinking pools will regularly dry out grid cells at the pool edges as the receding water line causes a retreat of the pool boundaries. As soon as one pool grid cell is predicted to become dry, all subadult mosquitoes are simply moved into the adjacent cells, concentrating larvae and pupae into remaining pool cells. Clearly, this will impact further development of the remaining subadult mosquitoes through the C coefficient of equation (15). Field observations show high spatial variability in larval density within each pool. Clusters of subadult mosquitoes populate certain areas. In the model, however, larval abundance is constant throughout each pooled grid cell. Within a multicell pool spanning several grid cells, the model allows heterogeneity in larval abundances between adjacent cells. This is consistent with field observations of spatial variability in larval abundance.

2.2.3. Adult-Stage Simulation

[40] After emergence from the pools, adult mosquitoes are tracked through space and time using an individual-based approach, in contrast to the compartmental structure of the aquatic-stage simulation. Each mosquito simulated to emerge into the model domain has an associated attribute matrix, as shown in Table 2. At each time step in the model, after the aquatic routine has been stepped to simulate newly emerging adult mosquitoes in the simulation, the mosquito matrix is updated. Elapsed times since significant events are updated, and X and Y position and behavior of the mosquito are updated on the basis of radial random walk motion, corrected for wind displacement and including representation of CO_2 plumes as a host-seeking cue, as described below.

[41] We assume the following sequence of behavioral events: host seeking, biting, resting, oviposition, and again host seeking to repeat the cycle until the mosquito dies. This involves several key parameters to simulate accurately the mosquito dispersal and interaction with its immediate environment. Most importantly, the nominal flight velocity per model time step strongly influences the degree of dispersal. Flight velocity is difficult to assign directly, primarily because of generally erratic flight paths. Straight-line velocity measured over a few seconds will differ greatly from averaged flight velocity over 1 h. We use a weighted random walk formulation for mosquito dispersal, corrected for CO_2 stimulated host seeking behavior, and a slight correction for wind influence. We assign flight velocity to match predicted dispersal to that witnessed by other authors for *An gambiae*. In a wet region of Tanzania, marked female *An gambiae* mosquitoes were tracked by *Gillies* [1961], from which he estimated the average flight range of adult *An gambiae* females as between 1 and 1.5 km. In addition, he suggested that the majority of mosquitoes stayed well within that distance of the village. Similar results were observed in Burkina Faso by *Costantini et al.* [1996b]. To be consistent with these recorded dispersals surrounding villages, we assume that hourly effective flight velocity follows a normal distribution centered at a mean of 15 m h^{-1} and standard deviation of 5 m h^{-1}. A low effective velocity (compared to straight-line velocity) over one time step integrates periods of short-term resting and flight direction changes. Direction of flight is assumed random outside of a threshold distance from human habitation. We assume that the random component of flight is slightly weighted by a direct flight toward human habitation, to account for visual cues of the mosquito when host seeking. The effect is a random movement with a varying degree of "pull," dependent on distance from the houses. The weighting of this visual cue compared to random dispersion is a model parameter.

[42] If an individual mosquito senses a CO_2 concentration of 0.01% above background, it flies up the concentration gradient of the plume [*Takken and Knols*, 1999]. The carbon dioxide plume is dependent on wind speed and direction for the area of interest. We model the CO_2 plume at each time

step, with exhaling human and animal agents in the model grid as CO_2 sources. This is done using the Gaussian dispersion equation:

$$C_{CO2} = \frac{Q}{2\pi u_w \sigma_y \sigma_z} \exp\left(-\frac{1}{2}\frac{y^2}{\sigma_y^2}\right) \cdot \left[\exp\left(-\frac{1}{2}\frac{(z-H_e)^2}{\sigma_z^2}\right) + \exp\left(-\frac{1}{2}\frac{(z+H_e)^2}{\sigma_z^2}\right)\right], \quad (16)$$

where C_{CO2} is the concentration of CO_2 [g m^{-3}] at any position x meters downwind of the source, y meters crosswind of the source, and z meters above the ground level; Q is the carbon dioxide exhalation rate [g s^{-1}]; u_w is the horizontal wind velocity along the plume centerline [m s^{-1}]; H_e is the height of the emission plume centerline above the ground [m]; σ_z is the vertical standard deviation of the emission distribution [m]; and σ_y is the horizontal standard deviation of the emission distribution [m].

[43] The horizontal and vertical dispersion is a function of atmospheric stability conditions and downwind distance [*Smith*, 1968]. We assume that stable atmospheric conditions prevail during the nighttime periods of high mosquito activity, owing to radiative cooling at the land surface under clear skies. From the work of *Smith* [1968], the horizontal and vertical dispersions for such conditions are given by

$$\sigma_y = 0.31x^{0.71}$$
$$\sigma_z = 0.06x^{0.71}. \quad (17)$$

Furthermore, we assume a height of 1.0 m at which mosquitoes sense the plume, and an emission height of 1.5 m. The source emission of carbon dioxide exhaled is assumed to be 275 mL min^{-1} per human, and that emitted by livestock is estimated at 3925 mL min^{-1} [*Kinsman et al.*, 1995]. The concentration of carbon dioxide at each time step and position in the model domain is calculated as the sum of the contributions of all exhaling members of the community. The plume dimensions and directions vary with wind speed and direction, and mosquito activity response to CO_2 cues therefore varies strongly throughout the model domain. The plume is always oriented directly downwind.

[44] *Anopheles gambiae s.l.* is nocturnal in feeding and oviposition habits [*Haddow*, 1954]. The model simulates the diurnal cycle, and allows mosquito activity only during the evening and nighttime hours. Anophelines are assumed to rest during the day, either in houses or in nearby vegetation.

[45] Bed net use is represented by a simple parameterization in the model. When a mosquito enters a model grid cell identified as containing human habitation, we assume that there is a certain probability of a blood meal being taken. We assume (for now) that this probability is 0.5. In a dense village environment, the population may not be very sensitive to this parameter owing to the dense clustering of villagers' houses which provide abundant blood meal opportunities. This parameter can be varied spatially or adjusted globally to reflect bed net use in the village.

[46] Figure 6 shows adult-stage model flow. The model cycles through each individual, assesses the mosquito's gonotrophic and infectious states and updates the mosquito attributes for infection and blood meals on the basis of interaction with the environment or human agents at that individual mosquito's location. Figure 6 displays the complete decision set each mosquito faces between emergence and oviposition, but each time step only allows events that occur within the flight range of one time step.

2.2.4. Mortality

[47] Macdonald demonstrated, using a modified version of Ross's groundbreaking model, that mosquito longevity is the most important variable in malaria transmission [*Macdonald*, 1957; *Ross*, 1911]. According to the model, a reduction in longevity reduces malaria transmission potential much more than the same percentage reduction in abundance. It is therefore important to simulate probabilistic death at each time step on the basis of all factors influencing longevity. As discussed above, environmental stresses affect mosquito longevity. We assume that longevity is independent of infected state.

[48] The model incorporates a daily survivability based on daily average temperatures. Above a 40°C daily average temperature threshold, anophelines cannot survive [*Craig et al.*, 1999; *Martens*, 1997]. The survivability dependence on daily average temperature follows the model developed by *Martens* [1997]:

$$p = \exp\left(\frac{-1}{-4.4 + 1.31T_d - 0.03T_d^2}\right), \quad (18)$$

where p is the daily survivability probability of each mosquito and T_d is the average temperature of the previous 24 h.

2.2.5. Egg Development and Extrinsic Incubation Period

[49] Egg development within the mosquito follows the temperature-dependent model of *Depinay et al.* [2004] as shown in equation (14). For details of the temperature-dependent development rate of eggs within the mosquito, the reader is referred to the work of *Depinay et al.* [2004]. Ambient temperature at the mosquito's location regulates this development rate. If the mosquito has finished the full gonotrophic (egg development) cycle, and it encounters a suitable water body, then it deposits a clutch of eggs to add to the subadult mosquitoes of various stages already present in that water body.

[50] Once an adult mosquito takes an infectious blood meal and becomes infected, the parasite advancement beyond the midgut and into the salivary glands as infectious sporozoites requires 111 degree days above 16°C [*Detinova*, 1962]. Because each individual mosquito tracks degree days since infection, infective status depends on a simple comparison of this value to 111. If the mosquito reaches this point, it becomes capable of malaria transmission to humans during subsequent blood meals. Once it has become infectious with sporozoites in the salivary glands, all subsequent bites from the mosquito are capable of transmitting malaria.

2.2.6. Human Agents

[51] The model simulates immobile human agents, representing village inhabitants. Several underlying assumptions govern human agent behavior. First, neither acquired immunity nor superinfection is incorporated in the model. Superinfection refers to the acquisition of multiple infec-

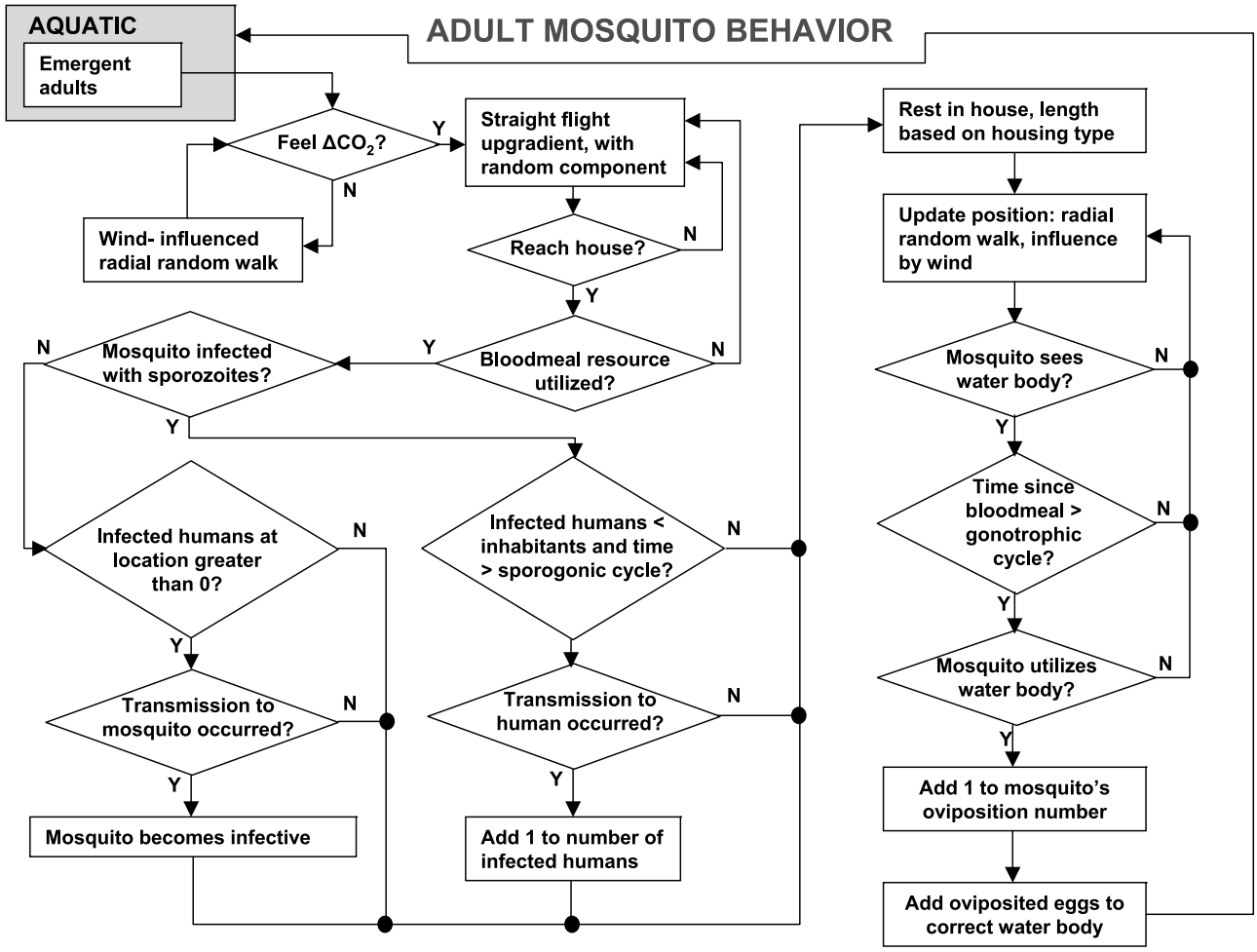

Figure 6. Adult mosquito simulation flow. Each model time step cycles through each mosquito, which may be at any point in this sequence of events.

tions of a single malaria species, which are independently cleared from the host with a first-order recovery rate [*MacDonald*, 1950]. Future research will investigate how human agents can be programmed to acquire immunity as a function of age and rate of infectious bites received. Similar alterations can be made for superinfection.

[52] Second, the human agents are assumed immobile. While villagers are obviously in reality quite mobile, this may be a reasonable assumption because the mosquitoes actively seek blood meal hosts at night [*Service*, 1993] when villagers are sleeping in their houses. Each model grid cell marked as inhabited (digitized houses from satellite image) contains a finite number of human agents. Unless house survey data allow actual assignment of inhabitant numbers to each house, we assume a constant 10 inhabitants per 10 m $\times$ 10 m village grid cell. When a mosquito enters a house to seek a blood meal, a certain portion of the inhabitants can be assumed protected by bed nets, and if that bed net–protected host is targeted by the mosquito for a blood meal it will result in the mosquito's death. If desired, repellent effects can also be included through a simple modification.

[53] Human agents track infected status as well as time since infection. Time since infection is tracked for gametocyte (parasite stage in humans which is infectious to biting mosquitoes) development and potential completion of the transmission cycle back to mosquitoes. Following an infectious mosquito bite, we assume that gametocyte development takes two weeks before a biting *Anopheles* mosquito can become infected. This intrinsic incubation period does not depend on ambient temperature, unlike the extrinsic incubation period of the parasite within the mosquito midgut. Human malaria infections are cleared with time. In the model algorithm, a uniform random number is chosen for each individual, which is compared to the preset clearing rate (adjusted for the hourly time step), and human infected status is toggled to negative if the random number is less than the clearance rate. This is a crude representation of human malaria infection, but the model framework as presented can easily be modified should improved algorithms for in vivo malaria dynamics become available.

2.2.7. Zoophily: Animal Agents

[54] A third type of agent can be represented in the model. Animals can act as alternate blood meal hosts, but cannot host infections of human malaria. Therefore, the presence of animals can divert potentially infectious bites from humans, with no negative consequence for either humans or mosquitoes. In other words, the mosquito's need for blood is satisfied, while parasite transmission is not advanced. In this way, higher animal densities can moderate

Table 3. Field Observations Taken in Banizoumbou Spanning the Period June 2005 to November 2006[a]

Variable	Sensor or Observation Mode	Sampling Frequency	Sampling Locations
Adult anopheline abundance	CDC light trap	weekly in wet season	six
Larval abundance	standard dipper	at least weekly	each pool
Pool dimensions	visual estimate	at least weekly	each pool
Precipitation	tipping bucket rain gauge	hourly	one meteo. station
Temperature	temperature/humidity probe	hourly	one meteo. station
Relative humidity	temperature/humidity probe	hourly	one meteo. station
Solar radiation	pyranometer	hourly	one meteo. station
Wind speed	anemometer	hourly	one meteo. station
Wind direction	wind vane	hourly	one meteo. station
Water temperature	HOBO Watertemp pro	hourly	one
Soil moisture	TDR probes buried	hourly	three (four sensors each location)

[a]CDC, Center for Disease Control. TDR, time domain reflectometry.

malaria transmission intensity in a village. *Anopheles gambiae s.s.* and *An. arabiensis* are predominantly anthropophilic, greatly preferring human blood to animal blood. There is some variation in anthropophily between the two malaria vectors simulated in the model, with *An gambiae* sensu stricto showing greater preference for human blood meals [*Coluzzi et al.*, 1979] and *An. arabiensis* showing less discriminating behavior. In West Africa, studies have shown *An. arabiensis* to be predominantly anthropophilic, except when near abundant alternative hosts, particularly cows [*Coluzzi et al.*, 1979; *Lindsay et al.*, 1993]. However, the degree of anthropophily in *An. arabiensis* can vary significantly by region, as evidenced by a finding of virtually complete zoophily in Madagascar [*Duchemin et al.*, 2001]. Exact levels of anthopophilic behavior are unknown in southwestern Niger. In the Sahel, animals are often found within the village at a low density where people keep their livestock near their homes, or near some of the largest water bodies at a higher density. Animal agents' locations are user-prescribed and are assumed immobile. The density per grid cell is a model parameter.

3. Field Data

[55] Hydrology and entomology data were collected from Banizoumbou starting in the 2005 wet season and continuing through the 2006 monsoon. Regular field observations of many hydrologic and entomologic variables were made. In addition, we logged meteorologic variables at Banizoumbou for model input. These data were collected at a meteorologic station located just outside of Banizoumbou village, in a sparse millet field. Meteorologic variables are considered invariant over the model domain. Table 3 summarizes the field data collected in Banizoumbou, and data collection locations for the study area are superimposed on a Quickbird satellite image of the village in Figure 7.

3.1. Adult Mosquito Abundance

[56] We monitored adult mosquito abundance weekly at six locations throughout Banizoumbou using Center for Disease Control (CDC) miniature light traps. These traps attract insects with a small 6-V incandescent bulb, and force insects near the bulb into a collecting net using a small fan. Trends in abundance follow trends in light trap captures, but absolute abundance values are difficult to establish using light traps. Sampling locations include four indoor and two outdoor light trap placements. The outdoor locations are outside the houses containing two of the light traps. Three of the sampled houses are mud-brick constructions with closed eaves and corrugated steel roofs, and one is built completely of thatch. Sampling locations remained unchanged throughout the June 2005 to November 2006 field observation period. For each sampling event, light traps were set with a freshly charged 6-V motorcycle battery, and started at 7 P.M. and stopped at 7 A.M. the following morning. The trap aperture was closed before the battery was removed. In the morning, the traps were removed, and all captured mosquitoes were separated from the other trapped organisms. All mosquitoes of genus *Anopheles* were identified to the species level, while other mosquito types were identified to the genus level. Light trap captures commonly included *Anopheles gambiae s.s.*, *An. arabiensis*, and rarely *An. rufipes* and *An. pharoensis*. *Mansonia*, *Culex* and *Aedes* mosquitoes were also commonly caught at all locations. Figure 8 (top) shows the *Anopheles gambiae s.l.* captures in Banizoumbou, summed over the six light traps operating in the village.

[57] The weekly CDC light trap mosquito capture data presented in Figure 8 display a pronounced dependence on lunar phase. The four indoor-placed traps showed only slightly less interweekly variability with the moon phase than the outdoor traps. The trap capture peaks are all within several days of a new moon, and the low captures correspond to full moons. Similar well-defined lunar cycle effects on anopheles mosquito light trap captures have been noted many times before [e.g., *Horsfall*, 1943; *Pratt*, 1948]. Moonlight competes with light trap bulbs as an attractant and mosquito flight stimulant, and on the brightest moonlit nights, moonlight may reduce the effective trap capture area dramatically because mosquitoes at some distance from the trap no longer resolve the bulb in the bright ambient light conditions. The reverse is true on moonless nights, when the light trap bulb attracts mosquitoes from a greater distance because the effect of the moon as a light source interfering with the light trap's illumination is no longer present. We account for the effects of lunar phase as follows. The light trap effective capture area is the annular area surrounding the trap where bulb illumination exceeds background illumination from the moon. The illumination of a light trap bulb (lux) is given by [*Bowden and Church*, 1973]

$$B = \frac{L}{D^2}, \tag{19}$$

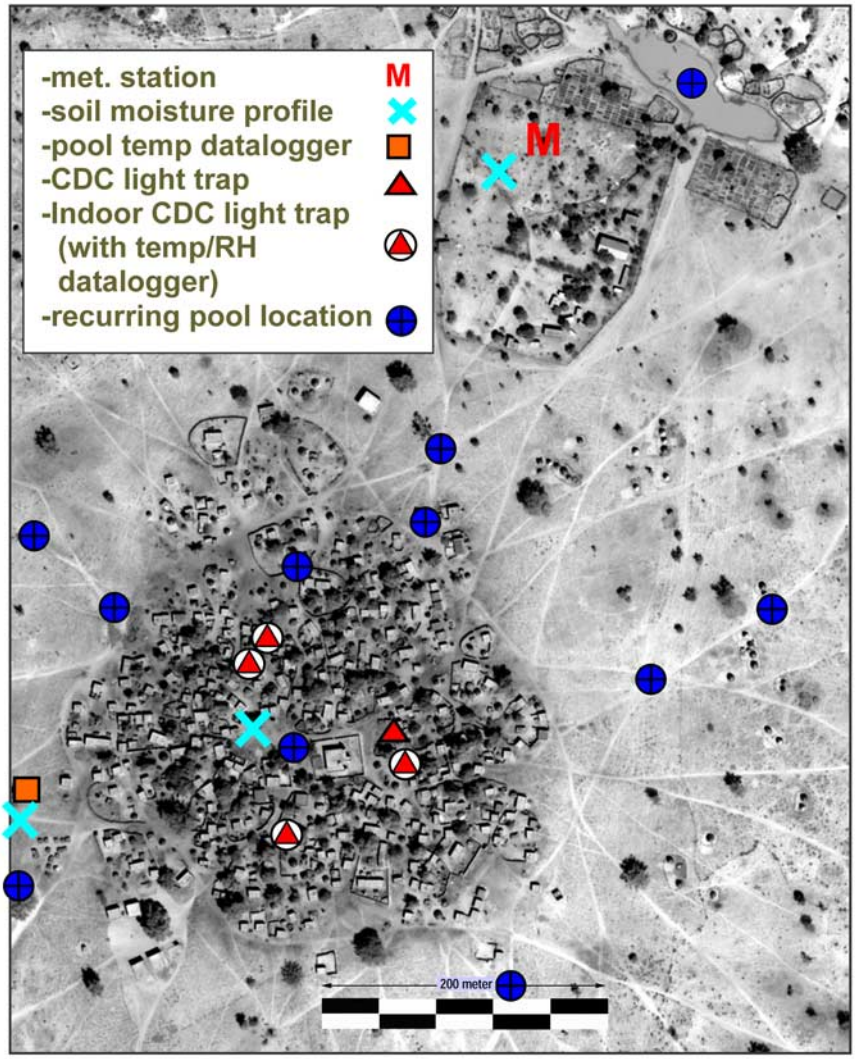

Figure 7. Sampling locations in Banizoumbou, Niger. CDC, Center for Disease Control. RH, relative humidity.

where L is the bulb intensity (lumens) and D is the radial distance from the trap (in meters).

[58] The value of D for which B matches the ambient moon light defines the radial extent of trap influence [*Service*, 1993]. Moonlight intensity is assumed to follow a sinusoidal pattern, with a maximum of 0.7 lx at full moon. A further sinusoidal correction to light intensity accounts for the proportion of each night with the moon above the horizon. At first quarter and last quarter the moon is only visible for half of the night.

[59] The expected catch in the trap's effective area can be expressed as the product of effective area and areal mosquito density:

$$M = \delta \cdot \pi D^2, \tag{20}$$

where M is the catch (mosquitoes) and δ is the density of mosquitoes (mosquitoes m^{-2}). Mosquito density is assumed independent of lunar phase and fluctuations in density are assumed attributable to environmental variables.

[60] Solving for δ, the relation becomes

$$\delta = \frac{B \cdot M}{\pi \cdot L}. \tag{21}$$

Background moonlight decreases to near zero at new moon, which according to equation (19) causes an unrealistically large D. We limit the possible effective radius of influence to 12 m to prohibit unrealistically low densities. Figure 8 (bottom) shows the corrected light trap captures, reformulated as areal mosquito density, independent of lunar phase.

3.2. Ephemeral Pool Observations

[61] We visited Banizoumbou at least twice weekly throughout each wet season to gather data. Soon after beginning regular sampling, it became evident where persistent and entomologically productive pools formed (see Figure 7). Each field visit involved inspection of these pool locations and a search for larvae. If water was present, then dimensions were estimated and larvae were sought. Standard entomologic dippers were used for larval counts, and the maximum of 10 successive dips was recorded. Other-

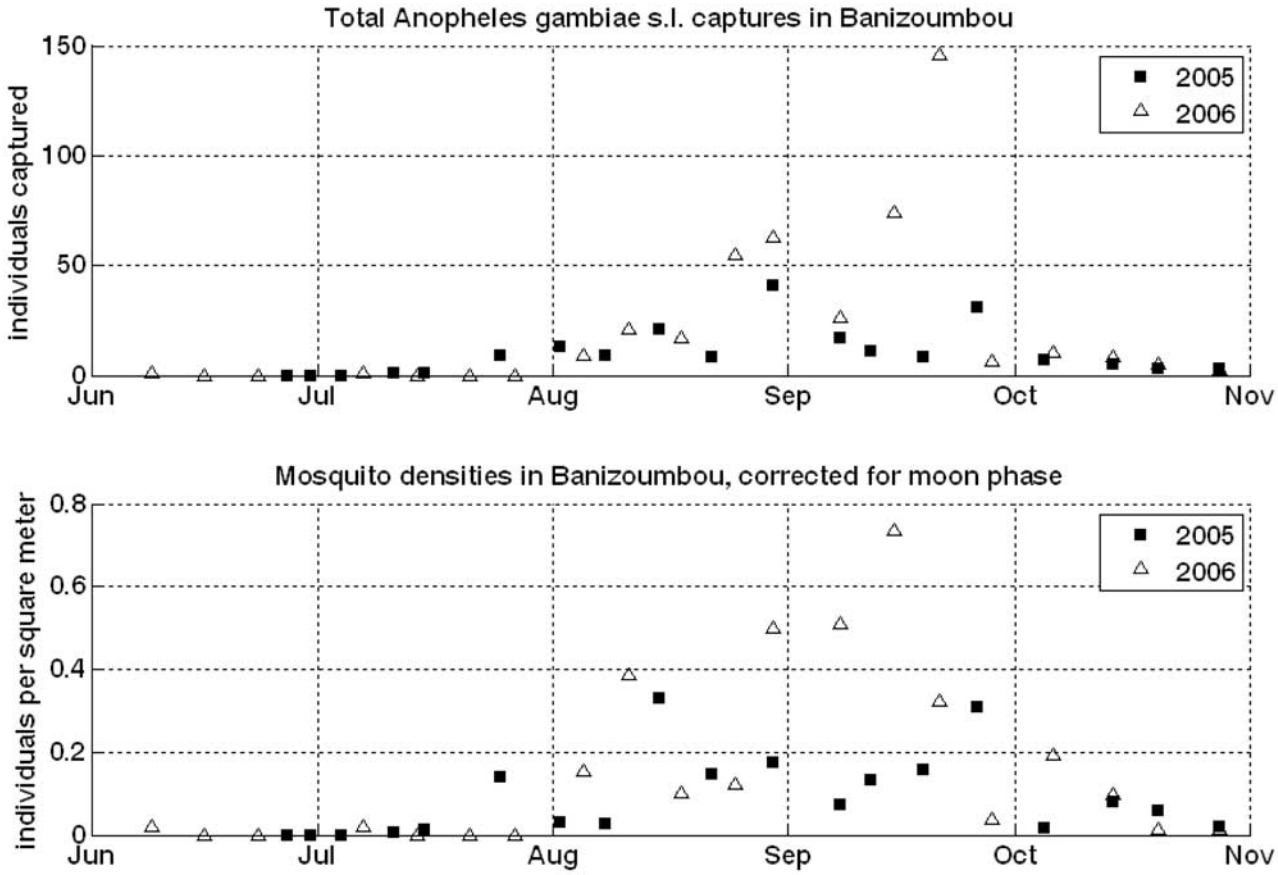

Figure 8. (top) *Anopheles gambiae s.l.* adult mosquito captures, summed over six light trap sampling locations in Banizoumbou. (bottom) Calculation of mosquito areal density to remove variability attributed to lunar phase effects.

wise, the location would be recorded as ''dry'' for that visit, and the pool considered devoid of larvae. In addition, we recorded water temperature, time of day, and turbidity at each sampling location, for each visit. Water temperature was measured in one ephemeral pool for several weeks using a HOBO Watertemp pro data logger (Onset Computer, Bourne, MA), until the sensor disappeared, likely picked up by curious passersby. In this manner, we carried out systematic monitoring of frequently recurring and persistent pools. Also, after large rainfall events, we conducted surveys to seek new pools that had not existed previously.

[62] The largest, most persistent pools in Banizoumbou did not always contain the most larvae and pupae. The establishment of predators after a certain period of pool existence can explain this counterintuitive observation. In addition, as previously mentioned, large pools tend to have small waves which may interfere with oviposition and the comfort of larvae at the pool shores. We observed the most larvae and pupae in newly formed, medium-sized (approx 20–30 m) pools.

3.3. Meteorology Measurements

[63] Precipitation, incoming shortwave radiation, temperature, humidity, wind speed and wind direction were sampled and recorded hourly at the Banizoumbou meteorological station (see location in Figure 7). The sensors are all at the same station site, and measurements are recorded using a Campbell Scientific CR10X data logger.

3.4. Soil Moisture Measurements

[64] We deployed three sets of four TDR soil moisture probes in and around Banizoumbou. These sensors measure volumetric water content at half-hour intervals, and the resulting values are recorded in data loggers for periodic download. These data are used for parameterization of the unsaturated zone hydrology model. The measurements began on 23 June 2005. Volumetric water content is measured at 10, 20, 50, and 100 cm from the surface in a vertical profile configuration. Diverse land cover types were chosen for TDR sensor locations: millet field, fallow field, and bare, compacted soil in the center of Banizoumbou village. These represent three of the predominant land cover types assigned to the model domain from remote sensing data.

4. Model Inputs and Grid

4.1. Parameterization: Hydrology Model

[65] As previously discussed, our modeling goal at Banizoumbou calls for us to simulate the pool water volume resulting from overland flow entering topographic depressions yielding suitable mosquito habitat, and the persistence of these pools after formation. This modeling goal requires

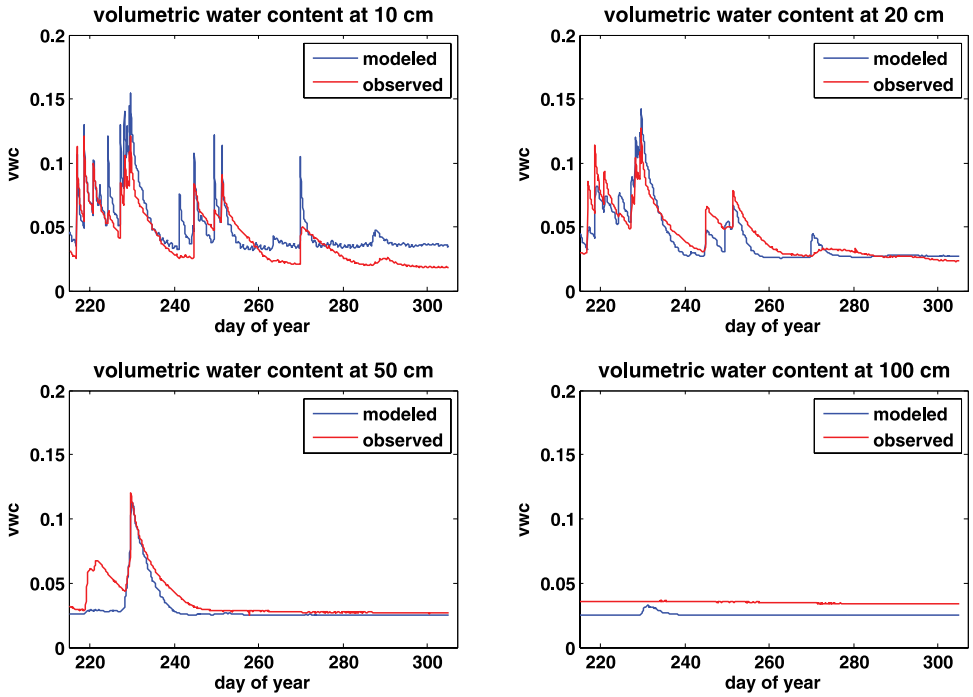

Figure 9. Model soil moisture output (volumetric water content) compared to measured soil moisture at a millet field 500 m north of Banizoumbou, for the period 1 August to 10 November 2005.

an accurate simulation of rainfall partitioning into runoff and infiltration at the soil surface, for determination of both the total runoff water entering a depression and the soil water dynamics in the unsaturated zone over the model domain. Soil moisture, which has significant "memory," will strongly influence runoff generation in the subsequent storm. This requires accurate parameterization of the unsaturated zone hydrology model to reproduce the temporal behavior of soil moisture in the vertical soil column as observed by the in situ soil moisture sensors.

[66] The model was calibrated for 2005 field data, and was subsequently verified with 2006 field data. The hydrology model was calibrated primarily for the vadose zone, but soil crusting was also represented. From the Richards equation and Campbell's formulation for soil water retention, the flexible, soil type–dependent model parameters are the air entry potential (ψ_e), saturated hydraulic conductivity (K_s), Campbell's curve fitting exponent (b), and porosity (θ_s). These four parameters for each discrete soil layer completely parameterize unsaturated zone water redistribution according to Campbell's model. With the addition of soil root zone uptake, all of the major determinants of soil moisture are modeled. This assumes homogeneous conditions in each layer and no lateral movement. Both of these assumptions are consistent with field observations of uniform sandy soils throughout the model domain. We assign parameter values to match model output to field observations, constrained by results of previous field investigations into soil characteristics at the site [*Peugeot et al.*, 2003; *Vandervaere et al.*, 1997]. Initial parameter assignments were made on the basis of typical values for the sandy soils of Banizoumbou and published values, and were refined using a Gauss-Newton method. The objective function for this optimization is formulated as a least squares minimization:

$$F(x) = \sum_{t=1}^{m} [y_t - h_t(x)]^2, \tag{22}$$

where y_t is observed soil moisture value at time t; h_t is simulated soil moisture value at time t, dependent on input parameters contained in vector x; F(x) is objective function value, as a function of parameter vector x; and m is total number of time steps.

[67] In the Gauss-Newton method, an approximation to the computationally expensive Hessian matrix is used, followed by a line search for a new estimated parameter set, for each iteration. This gradient-based methodology results in identification of local optima. We encountered the well-known topographic complexity of this objective function [*Lambot et al.*, 2002], and therefore began the Gauss-Newton search with published values for K_s and θ_s, and typical values for sand for ψ_e and b. A local optimum was found near these initial parameter values. While it was not evident if this local optimum was also a global optimum, within allowable ranges of parameters, Figure 9 represents the optimum. Figure 9 shows hydrology model fit with TDR soil moisture profile data at the "CFTEA" measurement site in Banizoumbou. Hydrology model parameterization is summarized in Table 4.

[68] The hydrology model operates on a rectangular grid. For the simulations at Banizoumbou presented here, we set up a 100 cell by 100 cell model domain centered on the village. The inner region of 10-m square cells is made up of 50 cells square, surrounded by ten 20-m-width cells on each side, then ten 40-m-width cells on each side, and finally five

Table 4. Hydrology Model Parameters, Including Saturated Hydraulic Conductivity K_s, Porosity θ_s, Campbell's "b" Exponent, Air Entry Potential Ψ_e, and Manning's n[a]

Parameter	Subsoil, All Classes	Surface Crust		
		Millet Field	Fallow	Pool Bottom
K_s	5.0×10^{-2} mm s^{-1}[b]	5.5×10^{-4} mm s^{-1}	1.9×10^{-3} mm s^{-1}[b]	1.7×10^{-4} mm s^{-1}
θ_s	0.3[b]	0.25	0.3[b]	0.3
B	2.9	6.0	6.0	7.6
Ψ_e	−0.98 J kg^{-1}	−2.84 J kg^{-1}	−2.84 J kg^{-1}	−3.63 J kg^{-1}
N	NA	0.12[c]	0.17[c]	0.05

[a]We use published parameters (when possible) for nominal values, which have been fine-tuned using a Gauss-Newton parameter estimation technique.
[b]From *Vandervaere et al.* [1997].
[c]From *Desconnets et al.* [1996].

cells around the outside of 80-m width. Thus, the total model domain has dimensions 2.5 km × 2.5 km.

[69] A land cover class was assigned to each cell. This was done by supervised classification of a Landsat 7 multispectral image [*Boyer*, 2003]. In the vicinity of Banizoumbou, the dominant land cover types of millet field, fallow field, and tiger bush shrubland were identified and assigned to each grid cell to parameterize root zone hydrology, transpiration, and surface roughness.

4.2. Parameterization: Entomology Model

[70] Table 5 summarizes entomological model parameters for the Banizoumbou simulation. Subadult-stage model parameterization generally follows that of *Depinay et al.* [2004]. The subadult model parameter values presented in Table 5 are chosen on the basis of other published models without field verification at Banizoumbou (e.g., ecological carrying capacity). Model parameterization was constant between the two years, so potential errors in some parameters are equally applied to the two years. A sensitivity analysis was performed for each parameter in Table 5, and its influence on peak mosquito abundance is represented in Table 5.

[71] On the basis of field observations of presence of cows, goats, and sheep near residences in Banizoumbou, we simulate one animal per village grid cell as a source of blood meals. Because we do not distinguish between *An. gambiae s.s.* and *An. arabiensis* as mosquito agents in the model, we assign a 10% chance of a blood meal being taken, should a blood-seeking mosquito encounter an animal. This value reflects the dominance of anthropophilic *An. gambiae s.s.* and the greater availability of human blood meals. Outside of village areas, for modeling purposes we assume there are no animals available for blood meals. This is supported by our observation that during the malaria transmission season, villagers prevent animals from roaming freely because they damage crops.

[72] In December 2005, Niger was the subject of a nationwide insecticide-treated bed net (ITN) distribution program. All families with children under 6 in Niger were given a free ITN from the program [*Loewenberg*, 2006]. In

Table 5. Entomology Model Parameterization

Variable	Nominal Value	Units	Reference[a]	Sensitivity[b]
Aquatic-Stage Simulation				
Cannibalism rate	0.0008	h^{-1}	7	medium
Number of eggs lain per oviposition	150		4	low
Egg death rate	0.001	h^{-1}	none	very low
Weight of first-stage larvae	0.02	mg	none	low
Weight of stage 2 larvae	0.16	mg	none	medium
Weight of stage 3 larvae	0.30	mg	none	medium
Weight of stage 4 larvae	0.45	mg	none	low
Lag time for predators to establish	240	h	2	low
Carrying capacity of pools	300	mg m^{-2}	2	low
Larvae death rate	0.005	h^{-1}	6	very low
Maximum predation rate for larvae	0.006	h^{-1}	2	medium
Pupae predation rate	0.005	h^{-1}	none	very low
Adult Mosquito Simulation and Human Individuals				
Human infection clearing rate	0.0005	h^{-1}	6	very low
Degree days above 18°C necessary for sporozoites	111	deg-day	3	very low
Probability that a mosquito takes a blood meal	0.07		none	low
Average mosquito flight velocity	15	m h^{-1}	1	low
Time required for gametocyte development	336	h	6	very low
Weighting of random walk versus straight line	0.2		none	medium
Resting time	24	h	none	medium
Threshold distance for visual cues	15	m	5	low
Utilization probability of water	0.95		none	low

[a]References are as follows: 1, *Costantini et al.* [1996b]; 2, *Depinay et al.* [2004]; 3, *Detinova* [1962]; 4, *Detinova and Gillies* [1964]; 5, *Gillies* [1980]; 6, *Hoshen and Morse* [2004]; 7, *Koenraadt and Takken* [2003].
[b]Parameter sensitivity gauged by maximum simulated abundance.

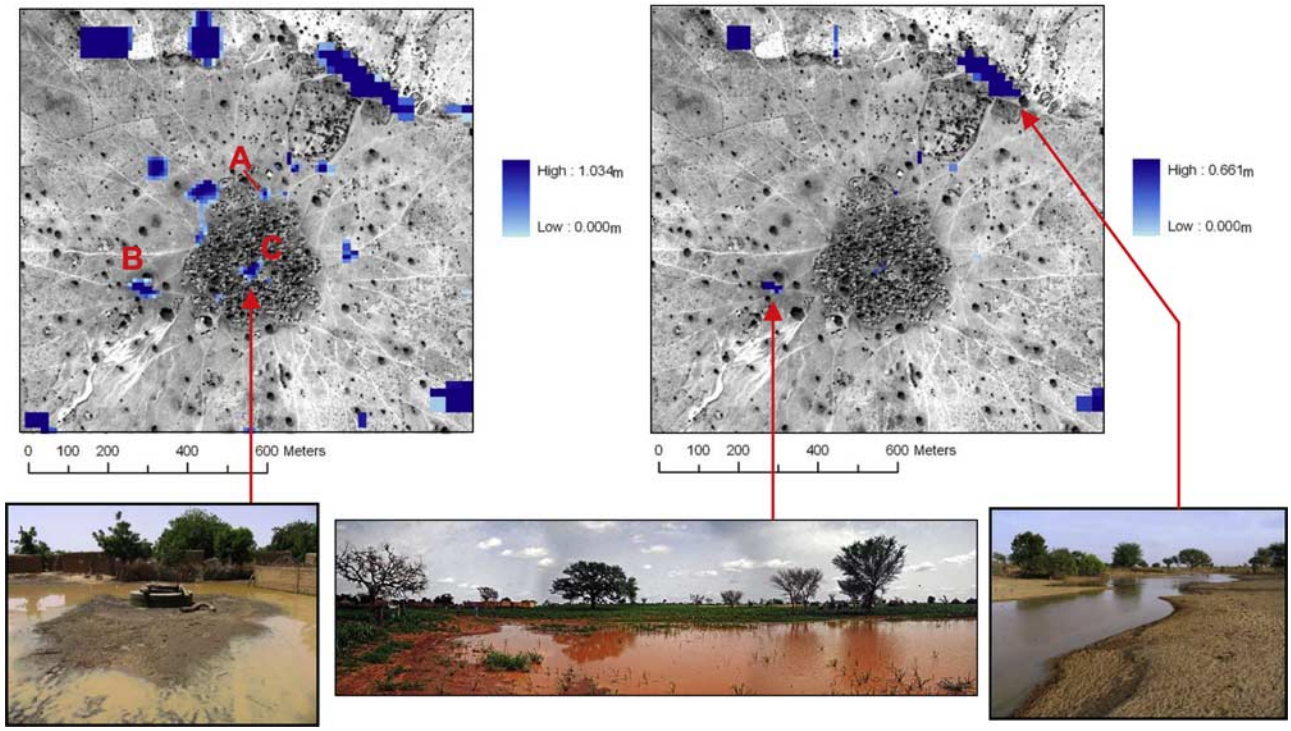

Figure 10. Two sample model output rasters for a subarea of the model domain, focused on Banizoumbou village. Each frame shows water depth above the ground surface in response to the 47-mm precipitation event of 11 August 2006, superimposed on a Quickbird satellite image. The frames represent water depths 2 days after the storm (left image) and 1 week after the storm (right image). Photos of the real pools corresponding to selected model-predicted pools are presented. The photos do not necessarily correspond to the same times as the model output in this figure. The locations "A," "B," and "C" identify locations of data presented in Figure 11.

Banizoumbou, we noted that 20% of all households were protected by an ITN as a result of the December 2005 bed net distribution. The permethrin-treated bed nets have a knockdown killing effect on mosquitoes attempting to feed on a sleeper under the net, and the resulting dramatic reduction in average daily survivability of a mosquito population makes ITNs highly effective for malaria control. We simulate the presence of bed nets in 2006 by killing a percentage of host-seeking mosquitoes entering houses with bed nets and attempting to feed. Not all mosquitoes simulated to enter an ITN-protected household will die. Because generally not all sleepers in the house are covered by an ITN, we assume that 80% of attempted blood meals are successful, because a repellent effect of the bed net may divert bites from protected individuals to unprotected inhabitants. The rest of the attempted blood meals result in the mosquito's death. ITN protection in houses is assigned randomly within the village so that the observed 20% coverage is attained. Mosquitoes that are in a village grid cell but are not seeking blood meal hosts are assumed to be flying past the houses and not entering, and are therefore not subject to the ITN's knockdown effect.

5. Results

5.1. Hydrology

[73] We simulate hydrology in Banizoumbou, Niger, for the 2005 and 2006 wet seasons. The 2005 wet season precipitation totaled 411.5 mm, and the 2006 wet season yielded 478.3 mm of rain, a 16% increase over the previous year. Much of the 2005 rainfall was unusually early and more sporadic than in 2006, when heavy rains started in mid-July and continued into September. The sporadic nature of the 2005 rainfall with greater between-storm durations allowed many pools to desiccate completely during the monsoon. This was not observed in 2006, and mosquito populations reflected this difference. Some 461 adults were captured in 2006 compared to 193 in 2005, a 140% increase. In both years we sampled the same locations with the same frequency, and the dramatic difference in observed mosquito populations evidently results from climatic variability between the two years.

[74] Figure 10 shows sample hydrology model results, superimposed on a 0.6-m resolution panchromatic Quickbird satellite image of Banizoumbou Village. The two frames show water depth in the model domain (Figure 10, left image) two days after the 47-mm precipitation event of 11 August 2006 and (Figure 10, right image) one week after the storm. No additional precipitation occurred during the week following this storm. In the succession of frames, water loss to evaporation and infiltration lowers the pool water levels. In this particular example, simulated evaporation flux in one depicted pool ranges from 0.1 to 5 mm d^{-1}, depending on temperature and humidity conditions. This is consistent with estimates by *Desconnets et al.* [1997] for a nearby pool in a similar village. As previously noted, pool

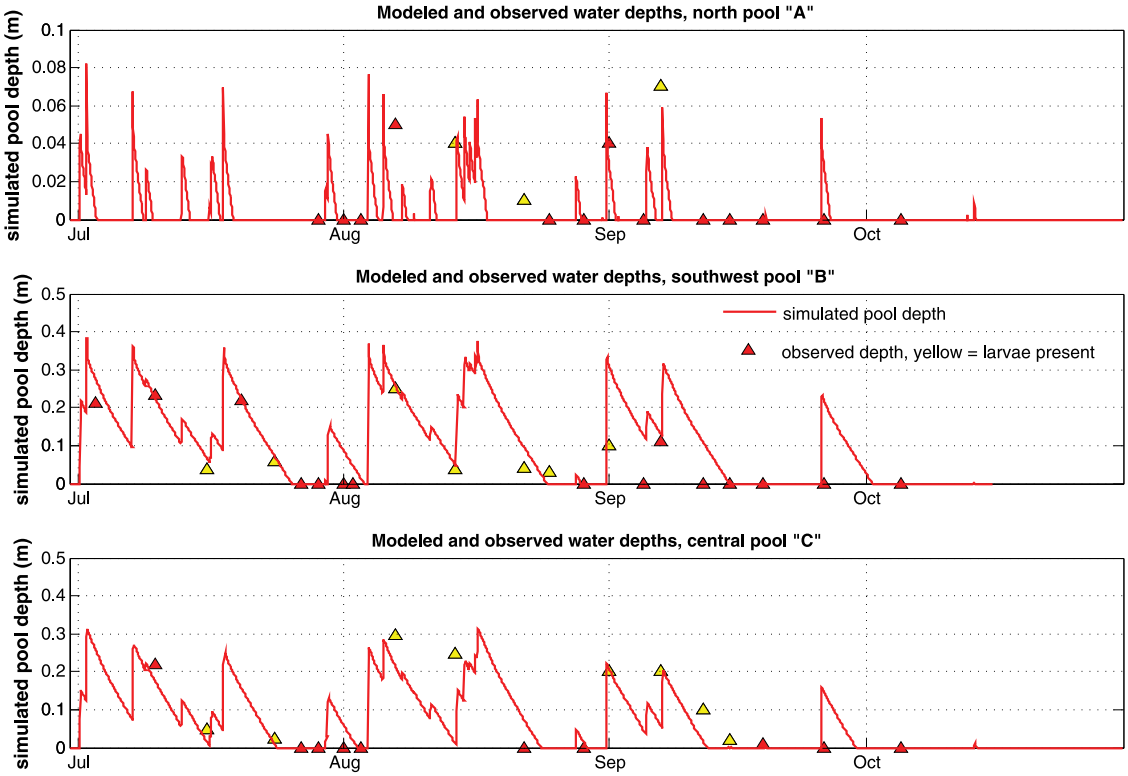

Figure 11. Simulated pool water levels for the 2005 rainy season at three pools in Banizoumbou (labeled "A," "B," and "C" in Figure 10) and larval presence at each field visit.

infiltration rates depend on water level, because the low-permeability substratum of clay-clogged sand in the pool bottoms inhibits pool infiltration losses up to a certain threshold pool water level [*Desconnets et al.*, 1997]. When the water level extends into sandy areas surrounding the pool, infiltration rates are high. Conversely, when it retreats to the clayey area, infiltration slows. We observe this characteristic in Banizoumbou pools, and therefore larger pools are assigned a lower top-layer saturated hydraulic conductivity on the basis of observed extents of clayey surface. As expected, water level recession rates for the example presented in Figure 10 are high because of the high infiltration rates occurring beyond the clayey zones. Infiltration at sandy pool edges dominates. Persistent, remnant pools in the clayey area are evident in the second frame.

[75] The persistent pooled areas are the most problematic because they allow uninterrupted mosquito breeding. Figure 11 plots modeled maximum pool depth over the 2005 wet season for three recurring productive pools of varying sizes. The plot includes depth estimates, which were calculated from a depth-area relationship using field-measured pool surface areas. The depth-area relationships were generated from very high resolution bathymetry data collected by topographic survey in December 2005, at approximately one meter resolution in the dry pool bottoms. Pool surface area measurements, made at each field visit with either a tape measure or a handheld GPS unit, contain some measurement error, estimated at about 10%, which would be carried over to the depth measurements as well. The southwest pool is shown in the photo of Figure 10. Pool size estimates and derived depths are reasonably well matched by the simulated pool depths for this sample of Banizoumbou pools. Notable deviations are evident in the southwest pool in September, which are not seen in the central pool. The primary reason for this disparity is the difference in land cover types within the catchments of each pool. The central pool, located in the center of Banizoumbou, catches water only from bare soil within the village, whereas the southwest pool catchment encompasses mostly cultivated millet fields. From field observations, crop height varies rapidly during the late growing season period, which is expected to result in a decrease of surface crusting from lower raindrop impact speeds and an increase of Manning's roughness parameter n from a greater vegetation density. Moreover, greater root zone uptake in the near-surface soil layers could be partly responsible for this, although such a signal is not evident in soil moisture measurements taken in millet fields. These temporal changes associated with crop growth are not incorporated in the hydrology model, and the result is an overprediction of pool depths in the southwest pool late in the growing season. The northern pool (labeled "A" in Figure 10), illustrates typical behavior of the smaller, more ephemeral pools surrounding Banizoumbou. Observations at this site are consistent with the simulated depths, except for one field visit in late August. In this case, pool surface area (about 10 m^2) was less than the model resolution, so failure to reproduce observed pool depth resulted from resolution limits. However, owing to their small overall size and highly ephemeral nature, resolution issues highlighted by the behavior of this pool are not expected to drastically influence entomology model results. We observed rapid pool drying after reaching such low levels. Observations of larval presence in the pool are shown in Figure 11, shown as yellow depth points. These

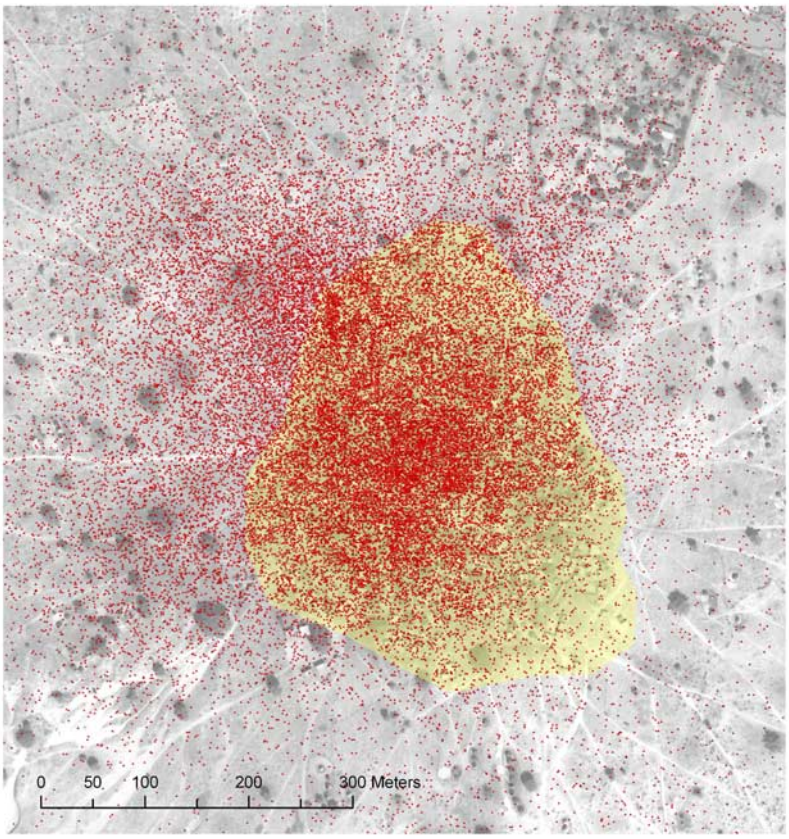

Figure 12. Example model output at an arbitrary time step. Image shows individual mosquitoes in red, superimposed on Banizoumbou Village (yellow buildings).

observations are for all larval instars, and in some cases only tiny first-stage larvae were observed after rewetting of a dried-out pool. Red points indicate an absence of larvae at that field visit.

[76] Larval counts were measured as the number of larvae caught in a standard dipper, and do not necessarily reflect abundance in the pools, because of clustering of the larvae. Certain areas of the pools typically had high larval density, whereas other sections of the same pool often had very low densities. Because of this problem, larval counts are not included on this plot and are replaced by an indication of larval presence at each field visit. When pools become completely dry, all larvae in those pools die. In this semiarid, hot and sunny region, mud rapidly dries, so potential interstorm survival of larvae in wet mud is unlikely. After desiccation, therefore, a pool will not yield adult mosquitoes for at least several days, until any deposited eggs in the rewetted pool have hatched and advanced through all of the subadult stages. The timing of adult emergence as allowed by persistent yet ephemeral pools, as shown by Figure 11, underscores the importance of precipitation timing. Sparse rainfall in short-duration low-intensity storms will not yield pools persistent enough to allow long uninterrupted periods of adult emergence. Therefore, this limitation in rainfall frequency, amount, and intensity will strongly affect population dynamics as shown in Figure 11 and the low 2005 mosquito capture data. Figure 11 is one example of pool behavior during the 2005 wet season. All pools in the simulation have similar dynamics in response to water inflows, and if sufficiently persistent the pools will control adult mosquito emergence comparably.

5.2. Entomology

[77] Emergent adult mosquitoes entering the model domain as mobile agents are faced with a series of environmentally influenced decisions. Carbon dioxide levels above background levels attract individual mosquitoes to human habitation, where they take human blood meals and make malaria transmission possible. Visual cues may also play substantial roles in host-seeking behavior. After biting and resting, mosquitoes seeking oviposition sites disperse from the village, and may utilize pools that they encounter. These behavioral processes suggest that close proximity to productive water body locations is an indicator of malaria risk, because mosquito densities are greater in houses near pools. This is indeed the case. *Minakawa et al.* [2002] observed that in a village in Western Kenya, 94% of captured anophelines were in houses within 300 m of the nearest productive breeding pools, 67% were in houses within 200 m, and 36.3% were in houses within 100 m of the nearest productive breeding site. Similar trends of decreasing biting rate with distance from breeding site are seen in data from the WHO Garki Project in Nigeria [*Molineaux and Gramiccia*, 1980]. Not enough houses were sampled in our study to draw similar conclusions in Banizoumbou. However, modeling results show a very similar effect. From the 2005 simulation, 99.6% of the simulated indoor-resting anophelines were in houses less than 200 m from the nearest productive

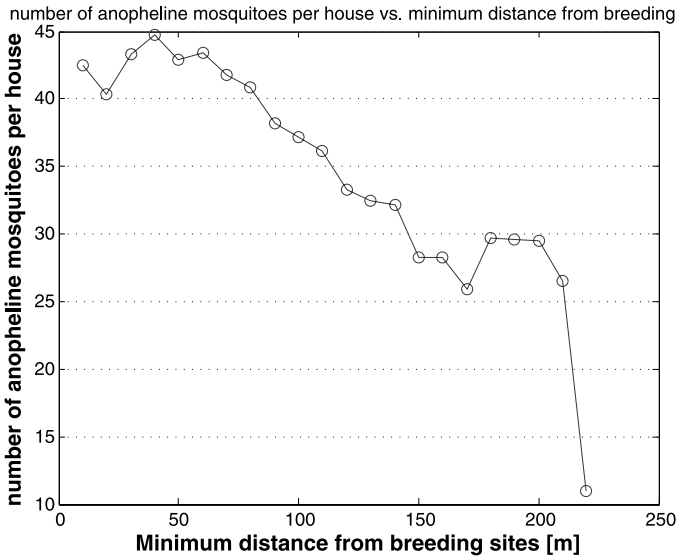

Figure 13. Model-predicted indoor resting density (mosquitoes per house) for the model output depicted in Figure 12.

breeding pool, 93% less than 150 m, and 67% were found less than 100 m from the nearest breeding habitat. These simulation results show a similar trend to that reported by *Minakawa et al.* [2002]; however, quantitative differences of simulation results with those of Minakawa are likely related to a different layout of the village as well as a different configuration of pools within the village. Figure 12 shows sample model output for one arbitrary time step during the peak of the 2005 transmission season. Dense clustering around the northeastern section of the village is compared to the southeast corner, where relatively few mosquitoes are seen. For this time step, average mosquito indoor resting density is plotted against distance from the nearest productive breeding site in Figure 13, showing the expected decrease as distance from breeding sites increases. Few houses are more than 250 m from the large, very productive pool near the well in the center of Banizoumbou. A major implication of spatial variability in mosquito density is the increased malaria transmissibility at certain locations within the village.

5.3. Mosquito Population Dynamics

[78] Simulated mosquito abundances are compared to observed trends using CDC light traps in Figure 14. The simulated mosquito abundances represent the total number of live mosquitoes over the whole model domain for each hourly time step. The result shows a general replication of trends and relative abundances (i.e., a strong wet-season peak in each year), however the simulated trends do not match the observed trends exactly on a weekly basis. It is likely that much of the discrepancy arises from limitations

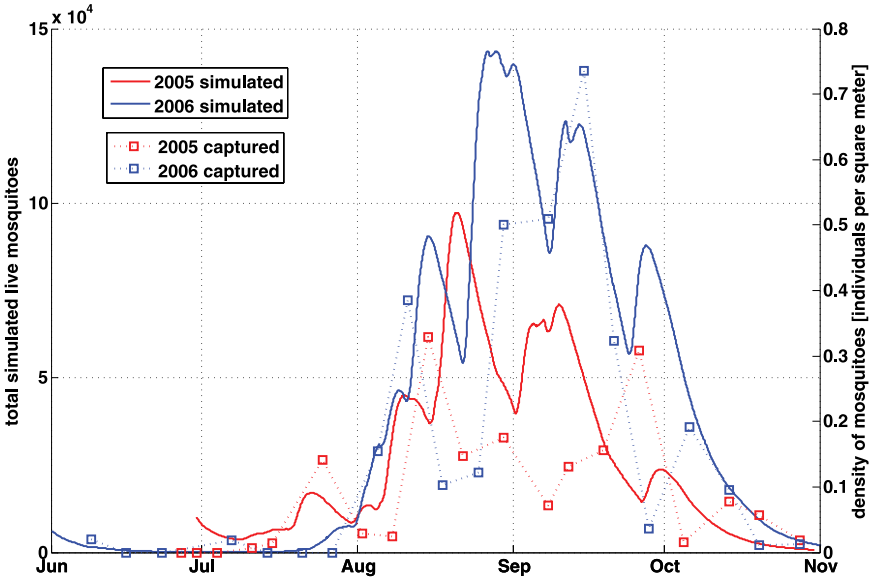

Figure 14. Simulated adult mosquitoes over the whole model domain in 2005 and 2006, compared to light trap captures in 2005 and 2006.

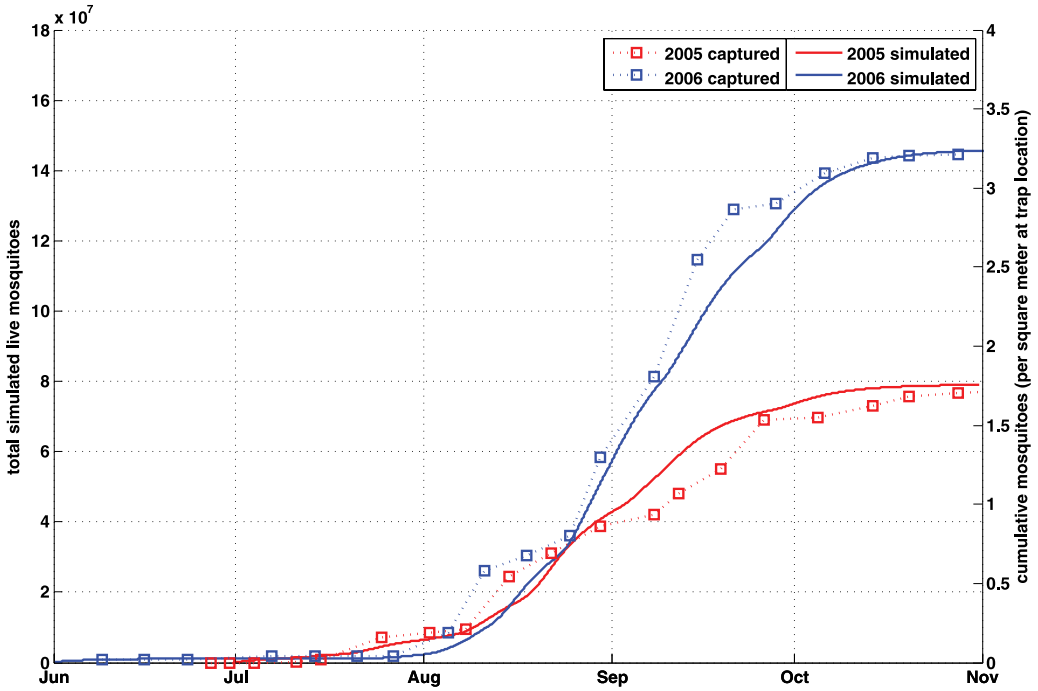

Figure 15. Cumulative mosquitoes, observed and model output.

of CDC light trap use. As previously discussed, it is difficult to relate catch numbers to abundance, primarily because of lunar phase effects. We have attempted a correction for lunar phase. However, the resulting comparison indicates that either additional measurement error in CDC light traps or the lack of highly specific details within the model governing the exact hourly behavior of simulated mosquitoes are sources of additional error. Nevertheless, light traps are valuable tools for measuring relative changes in abundance [*Service*, 1993]. As such, we compare cumulative simulated mosquitoes to cumulative mosquito captures in Figure 15. Relative differences in observed abundance between the two years are highlighted here. Model parameterization is unchanged between the two runs, except for the inclusion of ITNs. The increase derives solely from climatic variability between years, as ITNs would act to reduce abundances in 2006, compared to 2005 when they were absent from the village. The precipitation difference is a 16% increase between the two years, which is relatively small when compared to the more than doubling of mosquito populations. We attribute increased abundance to timing of rainstorms and resulting pool persistence. In 2005 the first rain fell in late April, which is unusually early for the area, and was spread out temporally with much of it in the form of local convection thunderstorms. Larger, organized mesoscale convective systems dominate precipitation in the peak of the monsoon and tend to yield more rain. These systems were more prevalent in 2006 than in 2005, which may partly explain the difference.

[79] In order to evaluate the sensitivity of predicted mosquito population dynamics to variations in individual parameters, we varied each model parameter by 5% and quantified the resulting response in mosquito population. The maximum seasonal abundance was used as a basis for comparison. Resulting model sensitivities are added as a column in Table 5. A multiplier of 1.05 was applied to each parameter, and the resulting effect on the mosquito abundance was assessed. Those parameters for which the predicted abundance increased 5% or less are denoted as having "low" impact, and those parameters for which the predicted abundance increased between 5% and 10% in response to the 5% parameter perturbation are denoted as having "medium" impact. We consider sensitivity of model outcome to parameters with a greater than 10% response of mosquito abundance to the 5% parameter perturbation as having a high impact. None of the model parameters in Table 5 matched this description.

5.4. Malaria Transmission

[80] The agent-based model simulates mosquito populations and their carriage and transmission of malaria parasite. Much focus in this paper has been on entomology simulation, primarily because model output can be compared to the entomological field data collected at Banizoumbou. We do not compare model simulations to malaria prevalence data. However, as previously discussed, many major steps in the malaria life cycle are represented: gametocyte development, uptake by blood-feeding mosquitoes, parasite development within the mosquito to the sporozoite stage, and subsequent inoculation of a human upon taking a second blood meal, provided the sporozoites are mature. As such, time series of malaria prevalence can be generated by the model. Predicted malaria prevalence for 2005 is presented in Figure 16. However, it should be emphasized that these data are not validated by field data and are merely presented to demonstrate this capability of the model. Malaria transmission simulation in no way influences the entomology simulation, so errors in malaria-related model parameters cannot affect the entomology

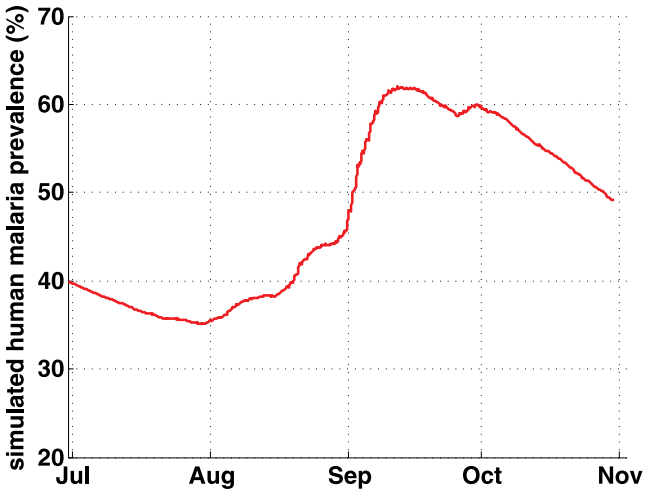

Figure 16. Model-predicted malaria prevalence.

model results. As previously mentioned, neither superinfection nor immune response as a function of inoculation rates are represented in the model.

6. Discussion

[81] In a water-limited environment such as the Sahel, land surface hydrology controls malaria mosquito population dynamics. In the case of Sahel malaria transmission, we have shown that high-resolution modeling yields credible, mechanistic modeling links of climate variable inputs to village-scale malaria transmissibility through hydrology and entomology model components. A variety of perturbations can be evaluated with the completed model. For example, land use changes, environmental management alterations, as well as climate variability and change scenarios can be explored by varying the inputs.

[82] The coupled model can be used to explore effects of land use change on malaria transmission. Land use changes in the Sahel have been noted with increasing population density. For example, *Leduc et al.* [2001] noted an unexpected rise in groundwater tables in southwestern Niger over the period of extended drought in the region in the last three decades. This apparently paradoxical result is attributed to land use changes associated with increasing rural population, and more land cleared for millet cultivation. This increases runoff coefficients to allow more runoff to reach topographic low points which in turn results in concentrated infiltration. *Leduc et al.* [2001] suggest that water distribution into pools is more dependent on land clearing by the rural population than on climate variability. This effect has obvious implications for pool persistence and associated mosquito breeding. With our hydrology model simulating overland flow over an infiltrating surface, such changes can be explicitly evaluated. High-resolution satellite multispectral images will allow the monitoring of such land use changes and assignment of distributed model parameters. Plant functional type assignments for model grid cells affect root zone uptake and vadose zone water redistribution. Water uptake from the root zone will influence infiltration and runoff from subsequent storms. Changes in root zone water uptake, soil crusting, and surface roughness associated with increased cultivated land will likely lead to pronounced variations in malaria prevalence. Future research using the presented model will address these questions.

[83] Similar to changes in distributed parameters, environmental management scenarios can be evaluated. Environmental management for mosquito abatement typically involves alteration of breeding habitats, such as pool filling or reshaping the bathymetry to make it less persistent or otherwise unfavorable for mosquito breeding. In the presented model, removal of specific pool locations can be incorporated by modification of the DEM. Larviciding can be simulated by allowing water to pool in the original depression, but raising larval mortality rates to reflect the larvicide's effects.

[84] Using the weekly CDC light trap catches in Banizoumbou as a comparison, the model has proven successful in simulating the variability of mosquito populations at seasonal and interannual timescales; however, at shorter timescales the model has limited ability to replicate trends in observations made by CDC light traps. We attribute this limitation to two factors. First, CDC light traps are not perfect sensors of absolute abundance at the sampling location, as discussed previously. Second, the assumption of spatial uniformity in atmospheric forcing may also influence spatial population distributions. Random error resulting from this assumption may be partially responsible for the discrepancies between simulation results and observations at weekly timescales. The potential importance of microhabitats for providing sheltered areas within houses, tree canopies, or other vegetation may be an important factor regulating short-timescale mosquito behavior. As presented, the model does not incorporate possible mosquito behavior leading to the utilization of such areas in which they are protected from adverse meteorological conditions. In response to microhabitat availability, resting behavior or flight paths may in fact deviate from the assumptions of fixed resting times and radial random walk which are presently incorporated into this model. Error resulting from such assumptions in the model, combined with random error in light trap measurements, likely result in the difference between observations and simulation results. At longer timescales, random errors are averaged out, resulting in better model correspondence to observations at seasonal to interannual timescales.

[85] As has been presented in this study, effects of interannual climate variability on malaria-transmitting mosquito population dynamics are evaluated within this modeling framework. An example of real interannual variability at Banizoumbou has been presented and has shown the importance of both timing and amount of precipitation for mosquito breeding, emphasizing the need for simulation at temporal scales which resolve individual storms. Hortonian runoff generation and overland flow over an infiltrating land surface into topographic depressions, as well as subsequent pool level recession are short-timescale processes. The timing of pool recession until desiccation exerts strong controls on mosquito development. For these reasons, imperfect matches of observed and simulated mosquito abundances at short timescales do not diminish the value and need for simulation at short timescales.

[86] Similar to climate variability evaluations, climate change scenarios can be simulated by changing climate inputs to the model. Climate change occurs over a long timescale, and so model assumptions of stationary and unvarying human populations may not completely reflect human adaptability to changes, but aside from this caveat, mechanistic modeling links between climate change and malaria transmission can be achieved using the presented model.

7. Conclusion

[87] The presented model provides a spatially explicit representation of Anopheles mosquito population interactions with humans and natural environments. It provides an organized, structured, and mechanistic means of representing known environmentally sensitive causations of malaria transmission. We have calibrated the model using observed field data from 2005, and have predicted 2006 hydrologic and entomologic conditions with the calibrated model. Distributed hydrology yielding favorable Anopheles mosquito breeding pools is successfully modeled in detail. The model successfully reproduces observed mosquito population dynamics at seasonal and interannual timescales, as well as spatial distributions of clustering near breeding pools and human habitation. However, at weekly timescales, limitations of the model become evident. It does not perfectly reproduce weekly CDC light trap measurements made at several locations within the village. This may reflect both deficiencies in CDC light traps as a short-timescale sampling method, as well as possibly some unknown short-timescale mosquito behavior governing exact distributions which the model does not include. Nevertheless, comparisons of time-integrated model output with observations confirm that climate variability controls on mosquito populations were successfully simulated. A 16% increase in rainfall between 2005 and 2006 was accompanied by a more than doubling in anopheline abundance, which the model reproduced. The presented model is also capable of tracking the acquisition and transmission of malaria parasite, and the temperature-dependent extrinsic incubation period. Future research will continue to develop the model and its applications.

[88] **Acknowledgments.** We would like to thank the villagers in Banizoumbou, Niger, for their cooperation with this field study. We also thank Luc Descroix of IRD in Niamey for invaluable field support and expertise on Niger Sahelian hydrology, and Ibrahim Issa-Arzika of CERMES, Niamey, for his assistance in field data collection and lab analysis of mosquito specimens. In addition, we acknowledge highly valuable discussions with the late Andrew Spielman. He and his colleague Tony Kiszewski provided much crucial entomology advice and guidance in the early stages of this research. Ali Sultan advised us on malaria dynamics and provided support in the early stages of the research as well. In addition, Wassila Thiaw of NOAA was instrumental in supporting this research. Financial support for this study came from the NOAA Oceans and Human Health Initiative.

References

Ahumada, J. A., D. LaPointe, and M. D. Samuel (2004), Modeling the population dynamics of Culex quinqefasciatus (Diptera: Culicidae), along an elevational gradient in Hawaii, *J. Med. Entomol.*, *41*(6), 1157–1170.

Amani, A., and T. Lebel (1996), Typology of rainfall fields to improve rainfall estimation in the Sahel by the area threshold method, *Water Resour. Res.*, *32*(8), 2473–2487, doi:10.1029/96WR01100.

Appawu, M., S. Owusu-Agyei, S. Dadzie, V. Asoala, F. Anto, K. Koram, F. N. Rogers, S. L. Hoffman, and D. J. Fryauff (2004), Malaria transmission dynamics at a site in northern Ghana proposed for testing malaria vaccines, *Trop. Med. Int. Health*, *9*(1), 164–170, doi:10.1046/j.1365-3156.2003.01162.x.

Bayoh, M. N., and S. W. Lindsay (2004), Temperature-related duration of aquatic stages of the Afrotropical malaria vector mosquito Anopheles gambiae in the laboratory, *Med. Vet. Entomol.*, *18*, 174–179, doi:10.1111/j.0269-283X.2004.00495.x.

Bowden, J., and B. M. Church (1973), The influence of moonlight on catches of insects in light-traps in Africa: part 2. The effect of moon phase on light-trap catches, *Bull. Entomol. Res.*, *63*, 129–142.

Boyer, L. (2003), *Rapport de Projet Pluridisciplinaire*, Ecole Natl. des Sci. Geogr., Marne-la-Vallee, France.

Campbell, G. S. (1985), *Soil Physics With BASIC*, 150 pp., Elsevier, New York.

Campbell, G. S., and J. M. Norman (1998), *Introduction to Environmental Biophysics*, 286 pp., Springer, New York.

Casenave, A., and C. Valentin (1992), A runoff capability classification system based on surface features criteria in semi-arid areas of West Africa, *J. Hydrol.*, *130*(1–4), 231–249, doi:10.1016/0022-1694(92)90112-9.

Charlwood, J. D., J. Kihonda, S. Sama, P. F. Billingsley, H. Hadji, J. P. Verhave, E. Lyimo, P. C. Luttikhuizen, and T. Smith (1995), The rise and fall of *Anopheles arabiensis* (Diptera: Culicidae) in a Tanzanian village, *Bull. Entomol. Res.*, *85*, 37–44.

Clements, A. N. (1963), *The Physiology of Mosquitoes*, 393 pp., Elsevier, New York.

Coluzzi, M., A. Sabatini, V. Petrarca, and M. A. Di Deco (1979), Chromosomal differentiation and adaptation to human environments in the Anopheles gambiae complex, *Trans. R. Soc. Trop. Med. Hyg.*, *73*, 483–497, doi:10.1016/0035-9203(79)90036-1.

Costantini, C., G. Gibson, N. Sagnon, A. Della Torre, J. Brady, and M. Coluzzi (1996a), Mosquito responses to carbon dioxide in a West African Sudan savanna village, *Med. Vet. Entomol.*, *10*(3), 220–227, doi:10.1111/j.1365-2915.1996.tb00734.x.

Costantini, C., S. Li, A. Della Torre, N. Sagnon, M. Coluzzi, and C. E. Taylor (1996b), Density, survival, and dispersal of *Anopheles gambiae* complex mosquitoes in a West African Sudan savanna village, *Med. Vet. Entomol.*, *10*(3), 203–219, doi:10.1111/j.1365-2915.1996.tb00733.x.

Costantini, C., N. F. Sagnon, A. della Torre, M. Diallo, J. Brady, G. Gibson, and M. Coluzzi (1998), Odor-mediated host preferences of West African mosquitoes, with particular reference to malaria vectors, *Am. J. Trop. Med. Hyg.*, *58*, 56–63.

Craig, M. H., R. W. Snow, and D. le Sueur (1999), A climate-based distribution model of malaria transmission in sub-Saharan Africa, *Parasitol. Today*, *15*, 105–111, doi:10.1016/S0169-4758(99)01396-4.

Depinay, J. M., et al. (2004), A simulation model of African *Anopheles* ecology and population dynamics for the analysis of malaria transmission, *Malar. J.*, *3*, 29, doi:10.1186/1475-2875-3-29.

Desconnets, J. C., B. E. Vieux, B. Cappelaere, and F. Delclaux (1996), A GIS for hydrological modeling in the semiarid, Hapex–Sahel experiment area of Niger, Africa, *Trans. GIS*, *1*(2), 82–94.

Desconnets, J. C., J. D. Taupin, T. Lebel, and C. Leduc (1997), Hydrology of Hapex-Sahel Central Super-Site: Surface water drainage and aquifer recharge through the pool systems, *J. Hydrol.*, *188–189*, 155–178, doi:10.1016/S0022-1694(96)03158-7.

Detinova, T. S. (1962), *Age Grouping Methods in Diptera of Medical Importance*, 216 pp., World Health Organ., Geneva.

Detinova, T. S., and M. T. Gillies (1964), Observations on the determination of the age composition and epidemiological importance of populations of Anopheles gambiae Giles and Anopheles funestus giles in Tanganyika, *Bull. World Health Organ.*, *30*, 23–28.

d'Herbès, J. M., and C. Valentin (1997), Land surface conditions of the Niamey region: Ecological and hydrological implications, *J. Hydrol.*, *188–189*, 18–42, doi:10.1016/S0022-1694(96)03153-8.

Duchemin, J.-B., J.-M. Leong Pock Tsy, P. Rabarison, J. Roux, M. Coluzzi, and C. Costantini (2001), Zoophily of *Anopheles arabiensis* and *An. gambiae* in Madagascar demonstrated by odour-baited entry traps, *Med. Vet. Entomol.*, *15*(1), 50–57, doi:10.1046/j.1365-2915.2001.00276.x.

Gillies, M. T. (1961), Studies on the dispersion and survival of Anopheles Gambiae Giles in east Africa: By means of marking and release experiments, *Bull. Entomol. Res.*, *52*, 99–127.

Gillies, M. T. (1980), The role of carbon dioxide in host-finding by mosquitoes (Diptera: Culicidae): A review, *Bull. Entomol. Res.*, *70*, 525–532.

Gillies, M. T., and B. DeMeillon (1968), *The Anophelinae of Africa South of the Sahara*, S. Afr. Inst. of Med. Res., Johannesburg.

Haddow, A. J. (1954), Studies of the biting habits of African mosquitoes: An appraisal of methods employed, with special reference to the twenty-four hour catch, *Bull. Entomol. Res.*, *45*, 199–242.

Healy, T. P., and M. J. W. Copland (1995), Activation of Anopheles gambiae mosquitoes by carbon dioxide and human breath, *Med. Vet. Entomol.*, *9*, 331–336, doi:10.1111/j.1365-2915.1995.tb00143.x.

Hoogmoed, W. B., and L. Stroosnijder (1984), Crust formation on sandy soils in the Sahel. I. Rainfall and infiltration, *Soil Tillage Res.*, *4*, 5–23, doi:10.1016/0167-1987(84)90013-8.

Horsfall, W. R. (1943), Some responses of the malaria mosquito to light, *Ann. Entomol. Soc. Am.*, *36*(1), 41–45.

Hoshen, M. B., and A. P. Morse (2004), A weather-driven model of malaria transmission, *Malar. J.*, *3*, 32, doi:10.1186/1475-2875-3-32.

Jepson, W. F., A. Moutia, and C. Courtois (1947), The malaria problem in Mauritius: The bionomics of Mauritian anophelines, *Bull. Entomol. Res.*, *38*, 177–208.

Kinsman, R., F. D. Sauer, H. A. Jackson, and M. S. Wolynetz (1995), Methane and carbon dioxide emissions from dairy cows in full lactation monitored over a six-month period, *J. Dairy Sci.*, *78*, 2760–2766.

Kiszewski, A., and A. Teklehaimanot (2004), A review of the clinical and epidemiologic burdens of epidemic malaria, *Am. J. Trop. Med. Hyg.*, *71*(suppl. 2), 128–135.

Koenraadt, C. J. M., and W. Takken (2003), Cannibalism and predation among larvae of the *Anopheles gambiae* complex, *Med. Vet. Entomol.*, *17*, 61–66, doi:10.1046/j.1365-2915.2003.00409.x.

Lal, W. (1998), Performance comparison of overland flow algorithms, *J. Hydraul. Eng.*, *124*(4), 342–349.

Lambot, S., M. Javaux, F. Hupet, and M. Vanclooster (2002), A global multilevel coordinate search procedure for estimating the unsaturated soil hydraulic properties, *Water Resour. Res.*, *38*(11), 1224, doi:10.1029/2001WR001224.

Le Barbé, L., and T. Lebel (1997), Rainfall climatology of the Hapex-Sahel region during the years 1950–1990, *J. Hydrol.*, *188–189*, 43–73, doi:10.1016/S0022-1694(96)03154-X.

Leduc, C., G. Favreau, and P. Schroeter (2001), Long-term rise in a Sahelian water-table: The Continental Terminal in south-west Niger, *J. Hydrol.*, *243*, 43–54, doi:10.1016/S0022-1694(00)00403-0.

Le Menach, A., F. E. McKenzie, A. Flahault, and D. L. Smith (2005), The unexpected importance of mosquito oviposition behaviour for malaria: Non-productive larval habitats can be sources for malaria transmission, *Malar. J.*, *4*, 23, doi:10.1186/1475-2875-4-23.

Lindsay, S. W., P. L. Alonso, J. Schellenberg, J. Hemingway, J. H. Adiamah, F. C. Shenton, M. Jawara, and B. M. Greenwood (1993), A malaria control trial using insecticide-treated bed nets and targeted chemoprophylaxis in a rural area of The Gambia, West Africa: 7. Impact of permethrin-impregnated bed nets on malaria vectors, *Trans. R. Soc. Hyg. Trop. Med.*, *87*, 45–51, doi:10.1016/0035-9203(93)90175-P.

Loewenberg, S. (2006), Niger welcomes largest bednet distribution in history, *Lancet*, *367*(9521), 1473, doi:10.1016/S0140-6736(06)68630-3.

MacDonald, G. (1950), The analysis of infection rates in diseases in which superinfection occurs, *Trop. Diseases Bull.*, *47*, 907–915.

Macdonald, G. (1957), *The Epidemiology and Control of Malaria*, 201 pp., Oxford Univ. Press, New York.

Martens, W. J. M. (1997), *Health Impacts of Climate Change and Ozone Depletion: An Eco-epidemiological Modeling Approach*, Maastricht Univ., Maastricht, Netherlands.

Minakawa, N., C. M. Mutero, J. I. Githure, J. C. Beier, and G. Yan (1999), Spatial distribution and habitat characterization of anopheline mosquito larvae in Western Kenya, *Am. J. Trop. Med. Hyg.*, *61*(6), 1010–1016.

Minakawa, N., P. Seda, and G. Yan (2002), Influence of host and larval habitat distribution on the abundance of African malaria vectors in Western Kenya, *Am. J. Trop. Med. Hyg.*, *67*(1), 32–38.

Minakawa, N., G. Sonye, M. Mogi, and G. Yan (2004), Habitat characteristics of *Anopheles gambiae s.s.* larvae in a Kenyan highland, *Med. Vet. Entomol.*, *18*(3), 301–305, doi:10.1111/j.0269-283X.2004.00503.x.

Minakawa, N., G. Sonye, and G. Yan (2005), Relationships between occurrence of *Anopheles gambiae* s.l. (Diptera: Culicidae) and size and stability of larval habitats, *J. Med. Entomol.*, *42*(3), 295–300, doi:10.1603/0022-2585(2005)042[0295:RBOOAG]2.0.CO;2.

Molineaux, L., and G. Gramiccia (1980), *The Garki Project*, 311 pp., World Health Organ., Geneva.

Muriu, S. M., E. J. Muturu, J. I. Shililu, C. M. Mbogo, J. M. Mwangangi, B. G. Jacob, L. W. Irungu, R. W. Mukabana, J. I. Githure, and R. J. Novak (2008), Host choice and multiple blood feeding behaviour of malaria vectors and other anophelines in Mwea rice scheme, Kenya, *Malar. J.*, *7*, 43, doi:10.1186/1475-2875-7-43.

Mutuku, F. M., J. A. Alaii, M. N. Bayoh, J. E. Gimnig, J. M. Vulule, E. D. Walker, E. Kabiru, and W. A. Hawley (2006), Distribution, description, and local knowledge of larval habitats of *Anopheles gambiae s.l.* in a village in western Kenya, *Am. J. Trop. Med. Hyg.*, *74*, 44–53.

Okech, B. A., L. C. Gouagna, G. F. Killeen, B. G. Knols, E. W. Kabiru, J. C. Beier, G. Yan, and J. I. Githure (2003), Influence of sugar availability and indoor microclimate on survival of *Anopheles gambiae* (Diptera: Culicidae) under semifield conditions in Western Kenya, *J. Med. Entomol.*, *40*(5), 657–663.

Pascual, M., and A. Dobson (2005), Seasonal patterns of infectious diseases, *PLOS Med.*, *2*(1), article e5.

Pascual, M., J. A. Ahumada, L. F. Chaves, X. Rodo, and M. Bouma (2006), Malaria resurgence in the East African Highlands: Temperature trend revisited, *Proc. Natl. Acad. Sci. U. S. A.*, *103*(15), 5829–5834, doi:10.1073/pnas.0508929103.

Patz, J. A., K. Strzepek, S. Lele, M. Hedden, S. Greene, B. Noden, S. Hay, L. Kalkstein, and J. C. Beier (1998), Predicting key malaria transmission factors, biting and entomological inoculation rates, using modeled soil moisture in Kenya, *Trop. Med. Int. Health*, *3*(10), 818–827.

Peugeot, C., B. Cappelaere, B. E. Vieux, L. Seguis, and A. Maia (2003), Hydrologic process simulation of a semiarid, endoreic catchment in Sahelian West Niger: 1. Model-aided data analysis and screening, *J. Hydrol.*, *279*, 224–243, doi:10.1016/S0022-1694(03)00181-1.

Pollard, D., and S. L. Thompson (1995), Use of a land-surface-transfer scheme (LSX) in a global climate model: The response to doubling stomatal resistance, *Global Planet. Change*, *10*, 129–161, doi:10.1016/0921-8181(94)00023-7.

Pratt, H. D. (1948), Influence of the moon on light trap collections of Anopheles albimanus in Puerto Rico, *J. Natl. Malar. Soc.*, *7*, 212–220.

Ross, R. (1911), *The Prevention of Malaria*, 2nd ed., John Murray, London.

Service, M. W. (1993), *Mosquito Ecology: Field Sampling Methods*, 2nd ed., 988 pp., Elsevier, New York.

Shaman, J., M. Stieglitz, C. Stark, S. Le Blancq, and M. Cane (2002), Predicting flood and swampwater mosquito abundances using a dynamic hydrology model, *Emerg. Infect. Diseases*, *8*, 6–13.

Smith, M. E. (Ed.) (1968), *Recommended Guide for the Prediction of the Dispersion of Airborne Effluents*, 85 pp., Am. Soc. of Mech. Eng., New York.

Sutherst, R. W. (2004), Global change and human vulnerability to vector-borne diseases, *Clin. Microbiol. Rev.*, *17*(1), 136–173, doi:10.1128/CMR.17.1.136-173.2004.

Takken, W., and B. Knols (1999), Odor-mediated behavior of afrotropical malaria mosquitoes, *Annu. Rev. Entomol.*, *44*, 131–157, doi:10.1146/annurev.ento.44.1.131.

Talbot, M. R. (1980), Environmental responses to climatic change in the West African Sahel over the past 20,000 years, in *The Sahara and the Nile: Quaternary Environments and Prehistoric Occupation in Northern Africa*, pp. 37–62, A. A. Balkema, Brookfield, Vt.

Taylor, C. E., Y. T. Touré, J. Carnahan, D. E. Norris, G. Dolo, S. F. Traoré, F. E. Edillo, and G. C. Lanzaro (2001), Gene flow among populations of the malaria vector, Anopheles gambiae, in Mali, West Africa, *Genetics*, *157*, 743–750.

Teklehaimanot, H. D., J. Schwartz, A. Teklehaimanot, and M. Lipsitch (2004), Weather-based prediction of *Plasmodium falciparum* malaria in epidemic-prone regions of Ethiopia: II. Weather-based prediction systems perform comparably to early detection systems in identifying times for interventions, *Malar. J.*, *3*, 44, doi:10.1186/1475-2875-3-44.

Thomson, M. C., S. J. Connor, N. J. Ward, and D. Molyneux (2004), Impact of climate variability on infectious disease in West Africa, *EcoHealth*, *1*, 138–150, doi:10.1007/s10393-004-0004-y.

Thomson, M. C., F. J. Doblas-Reyes, S. J. Mason, R. Hagedorn, S. J. Connor, T. Phindela, A. P. Morse, and T. N. Palmer (2006), Malaria early warnings based on seasonal climate forecasts from multi-model ensembles, *Nature*, *439*, 576–579, doi:10.1038/nature04503.

Toutin, T., and L. Gray (2000), State-of-the-art of elevation extraction from satellite SAR data, *ISPRS J. Photogramm. Remote Sens.*, *55*, 13–33, doi:10.1016/S0924-2716(99)00039-8.

Vandervaere, J.-P., C. Peugeot, M. Vauclin, M. Angulo Jaramillo, and T. Lebel (1997), Estimating hydraulic conductivity of crusted soils using disc infiltrometers and mini tensiometers, *J. Hydrol.*, *188–189*, 203–223, doi:10.1016/S0022-1694(96)03160-5.

White, G. B. (1974), Anopheles gambiae complex and disease transmission in Africa, *Trans. R. Soc. Trop. Med. Hyg.*, *68*(4), 278–301, doi:10.1016/0035-9203(74)90035-2.

World Health Organization (2005), World malaria report, Geneva, available at http://rbm.who.int/wmr2005/html/1-2.htm.

Ye-Ebiyo, Y., R. J. Pollack, A. Kiszewski, and A. Spielman (2003), Enhancement of development of larval *Anopheles Arabiensis* by proximity to flowering maize (Zea Mays) in turbid water and when crowded, *Am. J. Trop. Med. Hyg.*, *68*(6), 748–752.

A. Bomblies and E. A. B. Eltahir, Ralph M. Parsons Laboratory, Massachusetts Institute of Technology, 15 Vassar Street, Cambridge, MA 02139, USA. (bomblies@mit.edu)

J.-B. Duchemin, Centre de Recherche Médicale et Sanitaire, International Network of the Pasteur Institute, BP 10887 Niamey, Niger.